Analysis of Lossy Dielectric Optical Waveguides

Md. Rezaul Islam

DEPARTMENT OF ELECTRICAL AND ELECTRONIC ENGINEERING
BANGLADESH UNIVERSITY OF ENGINEERING AND TECHNOLOGY
March 2006

Analysis of Lossy Dielectric Optical Waveguides

by

Md. Rezaul Islam

A thesis submitted to the Department of Electrical and Electronic Engineering of
Bangladesh University of Engineering and Technology (BUET)
in partial fulfillment of the requirements for the degree of
MASTER OF SCIENCE IN ELECTRICAL AND ELECTRONIC ENGINEERING

DEPARTMENT OF ELECTRICAL AND ELECTRONIC ENGINEERING
BANGLADESH UNIVERSITY OF ENGINEERING AND TECHNOLOGY
March 2006

The thesis entitled "**Analysis of Lossy Dielectric Optical Waveguides**" submitted by Md. Rezaul Islam, Roll No.: 040006206P, Session: April 2000 has been accepted as satisfactory in partial fulfillment of the requirement for the degree of MASTER OF SCIENCE IN ELECTRICAL AND ELECTRONIC ENGINEERING.

BOARD OF EXAMINERS

1. ..... 25/3/06 .....
Dr. Md. Shah Alam — Chairman (Supervisor)
Associate Professor
Department of Electrical and Electronic Engineering
BUET, Dhaka-1000, Bangladesh.

2. .....
Dr. S. Shahnawaz Ahmed — Member (Ex-Officio)
Professor and Head
Department of Electrical and Electronic Engineering
BUET, Dhaka-1000, Bangladesh.

3. .....
Dr. Md. Abdul Matin — Member
Professor
Department of Electrical and Electronic Engineering
BUET, Dhaka-1000, Bangladesh.

4. .....
Dr. A. K. M. Akther Hossain — Member (External)
Associate Professor
Department of Physics
BUET, Dhaka-1000, Bangladesh.

Declaration

It is hereby declared that this work is done by me and the thesis or any part of it has not been submitted elsewhere for the award of any degree or diploma.

Signature of the candidate

Md. Rezaul Islam

(Md. Rezaul Islam)

Dedication

To my parents

Contents

List of Figures

List of Tables

Acknowledgements

It is a great pleasure of the author to acknowledge his respect and gratitude to his supervisor Dr. Md. Shah Alam, Associate Professor, Department of Electrical and Electronic Engineering, BUET for his continuous guidance, supervision and valuable constructive suggestions. His constructive suggestions and supply of research materials are gratefully acknowledged. His guidance and continuous encouragement in every aspect of this work is deeply appreciated. Without his whole-hearted supervision, this work would not have been possible.

The author is grateful to Dr. M. A Matin, Professor, Department of Electrical and Electronic Engineering, Bangladesh University of Engineering and Technology (BUET), for his encouragement and suggestions.

The author also pays his profound gratitude to his parents, wife, relatives and friends for their inspiration towards the completion of this work.

Finally, the author is grateful to Dr. S. Shahnawaz Ahmed, Head of the Department of Electrical and Electronic Engineering, Bangladesh University of Engineering and Technology (BUET), for providing microcomputer lab facilities. The author is also indebted to librarian and all staffs of the Department of Electrical and Electronic Engineering (BUET), for their cordial help and assistance.

Abstract

An efficient vector finite element method with the hybrid edge/nodal triangular element is described in this thesis for the analysis of dielectric optical waveguides with an emphasis to the analysis of loss. The hybrid type element (a combination of linear edge elements and quadratic nodal elements) are used in the work. The edge element models the transverse fields and nodal element model axial component of field variable. Thus, in the approach a true hybrid mode analysis is ensured. The undesired spurious (non-physical) solutions do not appear anywhere and the approach provides a direct solution for the propagation constant. Since the eigenvalue corresponds to propagation constant rather than frequency, the method can be easily applied to the analysis of lossy waveguides.

However in this work, an indirect approach based on perturbation technique is employed for the calculation of loss in optical waveguides. Here, lossless field solutions obtained from the finite element method are used in the perturbation equation to calculate loss in optical rib waveguides and rectangular dielectric waveguides. Furthermore, the method is very flexible and can handle a wide variety of problems having sharp metal and/or dielectric edges. The most important is that the sparsity and the bandedness of the matrices are maintained, so high speed computation with large sparse generalized complex eigenvalue problem is possible. But in the work, the need for solving complex eigenvalue problem is eliminated by using the perturbation formula. Finally, the accuracy of this approach is checked by comparing the propagation characteristics of step index dielectric optical waveguides with and without loss.

Chapter 1

INTRODUCTION

Computer modeling techniques that allow an accurate simulation of the behavior of real devices have become common and popular with the availability of cheaper and powerful computer resources. These simulation techniques, however, help and guide experimental researchers to conduct research on imaginary devices perfectly and conveniently.

The increasing complexity of modern devices in optics and microwaves rules out accurate analytical treatment and so it has maintained a critical demand for accurate and efficient computer modeling. This work is concerned with the 2-D analysis of longitudinally uniform waveguides which are the fundamental components of these devices. The method described in this thesis and its computer implementation are capable of calculating guided modes of various waveguides, however, a special attention has been given to the analysis of loss in dielectric optical waveguides. The analysis is restricted to two dimensions since the fields in these structures have the form $F(x,y)\exp(-\gamma z)$. Even though, one can think that a proper modeling of waveguide based devices require 3-D analysis, it is possible to predict the performance characteristics almost accurately by 2-D analysis also.

Material science and fabrication technology have advanced in recent years at an explosive rate, creating a strong interest in the possibility of extending and replacing with optical devices several functions traditionally performed by electronics. Day by day, new optical devices are being designed, investigated and demonstrated in research laboratories throughout the world. This development, combined with the rapidly increasing demand for more sophisticated and widespread telecommunication services, has put a very strong pressure on the continuous development of accurate and efficient methods for the analysis of the devices and systems involved.

1.1 OPTICAL WAVEGUIDES AND ANALYSIS TECHNIQUES

It is known that a waveguide is a physical medium or path which traps electromagnetic wave or light and guide it in a specific direction. Due to the physical phenomenon of total internal reflection electromagnetic wave or light can propagate through a physical medium with a little loss. Waveguide containing dielectric materials widely used from microwave to optical wavelength regions. No magnetic material is used to be present. Dielectric waveguides are fundamental components of devices and systems both in microwaves and optics, and as such, a full understanding of how electromagnetic waves propagate in complicated waveguide structures is essential. While in microwaves dielectric waveguides constitute only one of the types of waveguide in use, in optics they are practically the only form of the waveguiding structure. They play an essential role in optoelectronics, being in the form of optical fibres, fibre lasers and amplifiers or in integrated optics where most devices are made from optical waveguides of different configurations and properties [1]-[8].

A knowledge on the materials and fabrication technologies used to make integrated optical waveguides may give a better understanding of the practical demands for dielectric waveguide analysis. Materials such as gallium arsenide (GaAs), Indium phosphide (InP), lithium niobate ($LiNbO_3$), lithium tantalate ($LiTaO_3$), silica (SiO_2), polymers, organic materials, and varieties of compounds are widely used in integrated optics. Many of these materials are anisotropic, graded, lossless/lossy, sometimes nonlinear also. Fabrication techniques recently have become so flexible that materials with complex index profile can be developed and devices with complicated geometry can also be developed. Diffusion and implantation techniques can be used to alter the refractive index profile of a substrate material. Furthermore, deposition, growth, and etching techniques can be used to control the thickness and shape of material layers. Thus it is possible to produce waveguides and devices with a wide variety of complicated shapes and refractive index profiles [1], [5]-[6]. The index profile can be arbitrarily inhomogeneous, anisotropic and/or graded, and it leads most frequently to structures which cannot be studied analytically [1], [7]. Requirements for the analysis are also varied. First of all, it is often necessary to establish how many modes a waveguiding structure will support. Most applications will require the propagation

of one or two modes, and small changes in dimensions or refractive indices can frequently result in the structure being either cutoff or supporting more than the desired propagation modes. Secondly, it is often desirable to know the precise field distribution of the modes for the practical purpose. Thirdly, it is usually necessary to know the propagation constant of a mode in a waveguide and in some cases, quite accurately. For example, for many optical (and microwave) switching functions the operating principle is interference between two modes, and a precise knowledge of the difference between the propagation constants of two modes is necessary. This difference is usually a very small percentage of the value of the propagation constant, and so an accurate calculation is very important.

There are various types of waveguides used in optical integrated circuits [7]-[8]. Waveguides that trap the light only in the direction of its thickness (y direction) are called 2-D optical waveguides or slab optical waveguides. It allows light to spread in the horizontal direction (x direction). 2-D Optical waveguides could be of stepped index profile or graded index profile. On the other hand, a 3-D waveguide traps the light in both x and y direction. 3-D Optical waveguides could also be of stepped index or graded index profile. Waveguides in which refractive index changes in steps are called the step-index (SI) optical waveguides. On the other hand, waveguides in which the refractive index changes gradually are called graded-index (GI) optical waveguides. Here it may be mentioned that the effect of inter modal dispersion may be reduced through the use of graded-index (GI) waveguides. These are well discussed in [6]-[8].

There is growing emphasis on numerical methods for engineering analysis because frequently it is not possible to obtain analytical solutions for many practical problems. An analytical solution is a mathematical expression that gives the values of the desired unknown quantity at any point in the problem domain and for any value of the parameters of the problem, such as geometrical dimensions and material properties. In contrast, numerical methods usually provide an approximate solution only at a discrete number of points in the domain and for a pre-selected choice of parameter values. Each new choice will usually require a new calculation (a new 'numerical experiment'). However, analytical solutions can be obtained only for certain situations. For problems involving complex boundary conditions and material properties, one has to resort to numerical methods that

provide approximate, but satisfactory solutions. Although the finite element method is usually formulated by means of the classical Galerkin or the variational/Rayleigh-Ritz methods, its present success is fundamentally tied to the widespread use of computers. Its development has paralleled the advances in computer power and their widespread use and possesses certain characteristics that take the advantage of the special facilities offered by high-speed computers. With increasing computer power available in relatively small machines, reasonably large finite element solutions can now be achieved on widely used workstations and even PCs. For example, one can solve eigenvalue problems with matrix orders of more than ten thousand on a PC. In fact, many current workstations are much more powerful (in speed and memory size) than many mainframes of only a few years ago.

1.2 REVIEW OF LITERATURE FOR LOSSY WAVEGUIDES

In this section, we review a number of commonly used finite element formulations for the modal analysis of dielectric optical waveguides, particularly focussing on the recent development of methods to reduce or eliminate spurious solutions encountered in the vector finite element analysis of lossless and lossy optical waveguide problems [9]-[35]. Finite element formulations may be obtained in a number of ways: either directly from the differential or integral equations which define the problem or by using weighted residual methods or variational methods. However, it is advantageous to take a variational approach whenever possible, especially when one global parameter (*e.g.*, a capacitance, a resonant frequency or propagation constant) is needed. Weighted residual methods are specially useful in problems for which a variational expression is not readily available or easy to derive. They can indeed be applied to any boundary value problem with established differential equation.

In different finite element formulations the eigenvalue may correspond to ω^2 or γ^2. We can call the first type *frequency formulation* (or simply ω-formulation), where the eigenvalue is an explicit known function of ω; the second one is the *propagation constant formulation* (or simply γ-formulation), where the eigenvalue is an explicit known function γ. Usually the γ-formulation is desired for the analysis of lossy waveguides. One important drawback of using an ω-formulation in waveguide analysis is that it gives as a

result the frequency of each waveguide mode corresponding to a selected value of the propagation constant while in practice the problem is usually the reverse, that is, one is normally interested in finding the propagation constant (possibly complex) at a specified frequency. Consequently, when using this type of formulation, iterations are needed to solve a practical problem. In contrast, a γ-formulation solves directly for the propagation constant at a given frequency, avoiding unnecessary iterations.

Additionally, the presence of loss in the waveguide brings another, more important disadvantage of ω-formulations. In this type of formulation we need to specify numerical value of the propagation constant but in the general case of waveguides including materials with loss the propagation constant is complex (as it is too in the case of complex waves in lossless waveguides). This choice cannot be arbitrary, the real and imaginary parts of the chosen value for the propagation constant should be consistent with a real situation in order to find real solutions for the frequency. Then, due to the impracticality of finding a proper, consistent guess for complex propagation constant, only γ-formulations are applicable to waveguide problems with loss (or for the same reason, to the study of complex modes in lossless waveguides).

In the scalar FEM, a functional in terms of either E_Z or H_Z depending on the mode is used. Although a formulation based on single scalar quantity is inadequate for the inherently hybrid-mode spectrum of isotropic/anisotropic or genuinely two-dimensional, inhomogeneous waveguide problems, useful approximation can be found in the form of quasi-TEM, quasi-TE modes, depending on the type of waveguide structure or the propagating modes of interest. These approximations can be sufficiently accurate in many practical cases. However, this method can not be used directly for a lossy waveguide as in most cases they are based on frequency formulation.

To evaluate rigorously the propagation characteristics of an inhomogeneous and/or anisotropic waveguide, a vectorial wave analysis [11]-[15] is necessary, with at least two field components. These formulations are fundamentally more accurate than scalar forms since they can represent true hybrid modes in a general dielectric waveguide. Vector FEM

in terms of both the longitudinal electric and magnetic field components (E_z, H_z) have been used for analyzing various microwave and optical waveguides, including lossy waveguides [11]-[16]. But, this type of formulation is affected with the appearance of spurious solutions. In the full vector formulations, the method is based on the full vector **H** or **E**. The full vector **H** formulation has become the most common choice and has been used extensively in the solution of microwave and optical waveguides. The full vector magnetic field formulation leads to an eigenvalue equation with real symmetric matrices. The eigenvector corresponds to the unknown values of all three components of the magnetic field in all nodal points. The most serious difficulty in using some node-based vector FEM formulations is the appearance of spurious, non-physical solutions interspersed with the real solutions. To remove the spurious solutions, the penalty function method [11]-[12] was developed, where a penalty parameter is introduced in the formulation to give the variational expression a new shape, where the divergence-free condition is forced in the least square sense and the spurious solutions may be eliminated from the guided mode spectrum. However, this method cannot be used directly for the calculation of loss. Using the Galerkin method, Hayata *et al.* [17] derived an approach in terms of the transverse magnetic field components only, which can eliminate spurious solutions in the analysis of anisotropic loss less waveguides but at the considerable expense of losing the sparsity of the matrices. The same method was later extended to diagonal anisotropic and lossy waveguide problems [17]-[20], where a complex quadratic eigenvalue equation is solved. This problem then suffers from two major drawbacks: doubling the order of the matrices and, more importantly, the loss of sparsity of matrices which makes the method impractical. Most of the approaches have found some special applications and suffer from some unavoidable problems [21]-[23].

A revolutionary approach is that with edge elements [24]-[29]. A completely different way of alleviating the problem of spurious solutions is the application of edge elements [24]-[29]. In these cases, starting from the full vector **H** formulation, edge elements are used to represent the vector fields. The use of first order tangential elements to analyze lossless dielectric waveguides results in a much complicated calculation of the element matrices and from this, a complicated matrix eigenvalue problem emerges needing special treatment due to the singularity of the matrices. However, a combination of edge and nodal elements

as used by Koshiba and Inoue [26] have found great attention for the analysis of true hybrid modes in inhomogeneous waveguides. Here the edge elements are used to describe transverse fields and nodal elements for the longitudinal fields, thus true hybrid mode analysis is ensured. This approach can be used to calculate loss directly. However, they are computationally expensive as complex eigenvalue equations are solved to calculate loss directly.

1.3 OBJECTIVE OF THE WORK

The objective of this work is to develop an efficient system based on finite element method for the analysis of lossy dielectric optical waveguides. Modal loss in dielectric optical waveguides will be calculated in this work by using a vector finite element method (VFEM) with the incorporation of the perturbation formula [43], [46]-[47]. The VFEM with the magnetic field intensity vector as the working variable with the hybrid type triangular elements [43] will be used to find the modal solutions of lossless waveguides. With the hybrid elements, the edges model the transverse fields ensuring tangential continuity along the element interfaces and nodes model the axial fields and thus the approach ensure true hybrid mode analysis. As the edges assign the degrees of freedom to the edges, they allow the field to change its direction abruptly and thus are capable of modeling the field properly at sharp dielectric edges at which field changes abruptly. The lossless field solutions will be employed in the perturbation formula [46]-[47] to calculate loss. The final global real eigenvalue equation of the VFEM approach will be solved using sparse eigenvalue solver. The approach thus eliminates the need for solving complex eigenvalue equation when a complex solver is unavailable and is capable of providing high-speed calculation of modal losses of dielectric optical waveguides. As examples, loss in rib waveguide and embedded channel waveguide will be investigated.

1.4 LAYOUT OF THE THESIS

This first chapter has included an overview to the background of currently used dielectric waveguides and a brief introduction to the fundamental features of the finite element method leading to justification of the need to develop a better finite element method for

lossless as well as lossy dielectric optical waveguide problem. This chapter contains a discussion on numerical methods and different finite element approaches for this purpose. A review of published finite element formulations for electromagnetic waveguide problems, particularly focussing on the recent development of methods to suppress or eliminate spurious solutions encountered in vector finite element analysis of waveguide problems are also discussed in this chapter. The difficulties of finite element method and the use of hybrid approach is also discussed in this chapter.

In chapter 2, basic theory related to the optical waveguide is discussed. Formation of modes and their modal designations are also given for better understanding of optical waveguides. In chapter 3, the basic idea of the finite element method is given. The historical background, the range of applications, basic steps of finite element formulations, and the solution procedures of the final system of equations are discussed in this chapter.

In chapter 4, the mathematical formulation with the hybrid edge/nodal element for the waveguide problem is discussed in details. The use of hybrid edge/nodal element to suppress the problems of spurious solutions and finite element discretization procedure is discussed in this chapter. The details of the shape function vector, elemental equations, the final equations for final matrix construction are also shown here in this chapter. This chapter also shows the perturbation procedure to calculate loss of optical waveguides.

Chapter 5 discusses on numerical results. The results are given here for optical rib and rectangular type waveguides. Both the lossless propagation characteristics and loss or gain characteristics are shown. A comparison between the existing results and the present results is also shown there. A brief description of the program is also given in this chapter. Finally, chapter 6 gives the conclusion of this work, where the findings are described briefly and future scopes related to this work are described. At the end, references related to this work and an appendix is given also.

Chapter 2

THEORY OF OPTICAL WAVEGUIDE

The basic concepts and equation of electromagnetic wave theory required of the comprehension of light wave propagation in optical waveguides are qualitatively explained, taking the case of a slab waveguide [1], [6]. Maxwell's equations, boundary conditions, and complex Poynting vectors are described as they form the basis for the waveguiding mechanism in the dielectric optical waveguides.

2.1 WAVEGUIDE STRUCTURE

Optical fibers and optical waveguides consist of a core, in which light is confined, and a cladding, or substrate surrounding the core, as shown in Fig. 2.1. The refractive index of the core n_1 is higher than that of the cladding n_0. Therefore the light beam that is coupled to the end face of the waveguide is confined in the core by total internal reflection. The condition for the total internal reflection at the core-cladding interface is given by $\sin(\pi/2-\phi) \geq n_0$. Since the angle ϕ is related with the incident angle θ by $\sin\theta = \sin\phi \leq \sqrt{n_1 - n_0}$. We obtain the critical condition for the total internal reflection as

$$\theta \leq \sin^{-1}\sqrt{n_1^2 - n_0^2} \equiv \theta_{\max} \tag{2.1}$$

The refractive index difference between core and cladding is of the order of $n_1 - n_0 = 0.01$

Then $\theta_{\max}$ in equation (2.1) can be approximated by

$$\theta_{\max} \cong \sqrt{n_1^2 - n_0^2} \tag{2.2}$$

$\theta_{\max}$ denotes the maximum high acceptance angle of the waveguide and is known as the numerical aperture (NA). The relative refractive index difference between n_1 and n_0 is defined as

$$\Delta = \frac{n_1^2 - n_0^2}{2n_1^2} \cong \frac{n_1 - n_0}{n_1} \tag{2.3}$$

Δ is commonly expressed as a percentage. The numerical aperture NA is related to the relative refractive index difference Δ by

$$\text{NA} = \theta_{\max} \cong n_1\sqrt{2\Delta} \tag{2.4}$$

The maximum angle for the propagating light within the core is given by $\phi_{\max} \cong \theta_{\max} / n_1 \cong \sqrt{2\Delta}$. For typical optical waveguides, NA=0.21 and $\theta_{\max} = 12°$ ($\phi_{\max} = 8.1°$) when n_1=1.47, $\Delta = 1\%$ (for n_0=1.455).

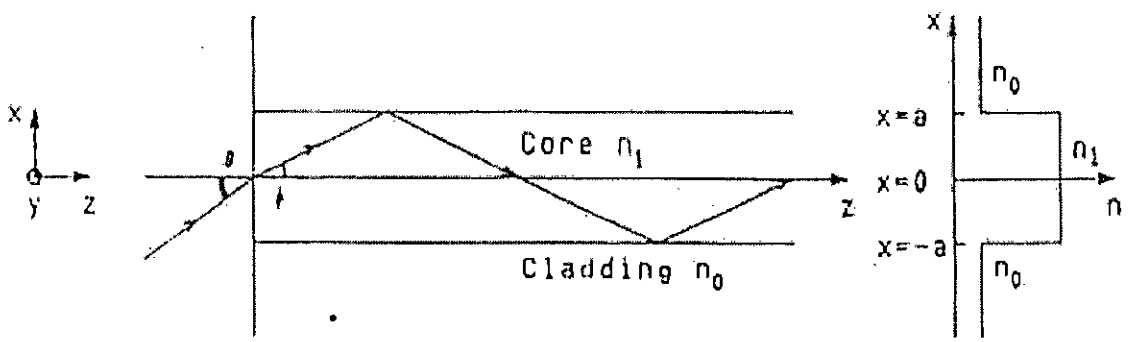

Fig. 2.1: Basic structure and refractive index profile of the optical waveguide.

2.2 FORMATION OF GUIDED MODES

We have accounted for the mechanism of mode confinement and have indicated that the angle ϕ must not exceed the critical angle. Even though the angle ϕ is the smaller than the critical angle, light rays with arbitrary angles are not able to propagate in the waveguide. Each mode is associated with light rays at a discrete angle of propagation, as given by electromagnetic wave analysis. Here we describe the formation of modes with the ray picture in the slab waveguide [6], as shown in Fig. 2.2. Let us consider a plane waves propagating along the z-direction with inclination angle ϕ. The phase fronts of the

plane waves are perpendicular to the light rays. The wavelength and the wavenumber of light in the core are λ / n_1 and $kn_1 (k = 2\pi / \lambda)$ respectively, where λ is the wavelength of light in vacuum. The propagation constants along z and x (lateral direction) are expressed by

$$\beta = kn_1 \cos\phi \tag{2.5}$$

$$\kappa = kn_1 \sin\phi \tag{2.6}$$

Before describing the formation of modes in detail, we must explain the phase shift of light ray that suffers total reflection. The reflection coefficient of the totally reflected light, which is polarized perpendicular to the incident plane (plane formed by the incident and reflected rays) as shown in Fig. 2.3, is given by [6]

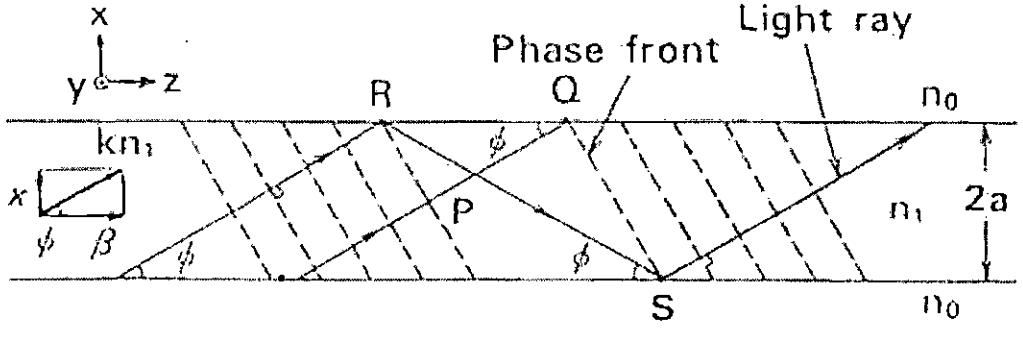

Fig. 2.2: Light rays and their phase fronts in the waveguide.

$$r = \frac{A_r}{A_i} = \frac{n_1 \sin\phi + j\sqrt{n_1^2 \cos^2\phi - n_0^2}}{n_1 \sin\phi - j\sqrt{n_1^2 \cos^2\phi - n_o^2}} \tag{2.7}$$

when we expressed the complex reflection coefficient r as $r = \exp(-j\phi)$, the amount of the phase shift ϕ is obtained as

$$\phi = 2\tan^{-1}\frac{\sqrt{n_1^2 \cos^2\phi - n_o^2}}{n_1 \sin\phi} = -2\tan^{-1}\sqrt{\frac{2\Delta}{\sin^2\phi} - 1} \tag{2.8}$$

where (2.3) has been used. The forgoing phase shift for the totally reflected light is called the Goos-Hanchen shift [1], [6].

Let us consider the phase difference between the two light rays belonging to the same plane wave in Fig. 2.2. Light ray PQ, which propagates from point P to Q, does not suffer the influence of reflection. On the other hand, light ray RS, propagating from point R to S, is reflected two times (at the upper and lower core cladding interfaces). Since points P and R or points Q and S are on the same phase front, optical paths PQ and RS (including the Goos-Hanchen shifts caused by the two total reflections) should be equal, or their difference should be an integral multiple of 2π. Since the distance between points Q and R is $2a/\tan\phi - 2a\tan\phi$, the distance between points P and Q is expressed by

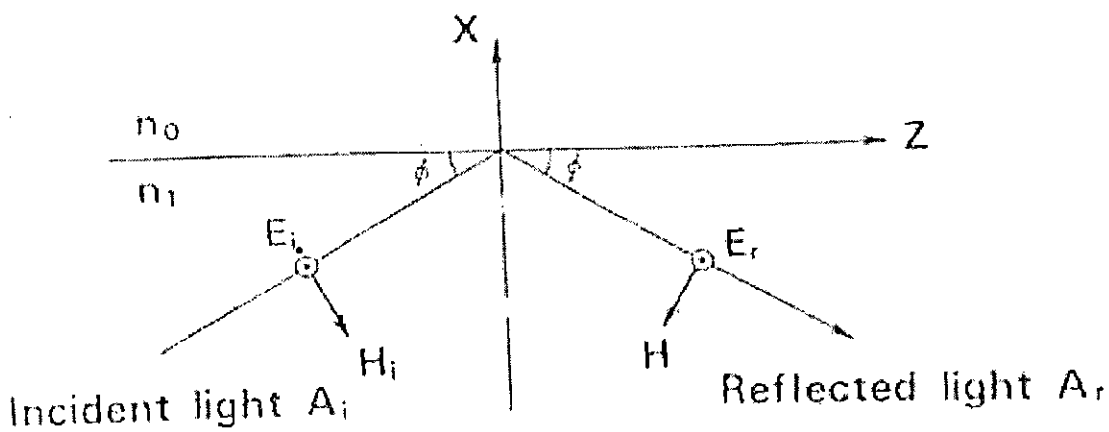

Fig 2.3: Total reflection of a plane wave at a dielectric interface.

$$\ell_1 = \left(\frac{2a}{\tan\phi} - 2a\tan\phi\right)\cos\phi = 2a\left(\frac{1}{\sin\phi} - 2\sin\phi\right) \tag{2.9}$$

Also, the distance between points R and S is given by

$$\ell_2 = \frac{2a}{\sin\phi} \tag{2.10}$$

The phase matching condition for the optical paths PQ and RS then becomes

$$\left(kn_1 l_2 + 2\Phi\right) - kn_1 l_1 = 2m\pi \tag{2.11}$$

where m is an integer, Substituting (2.8)–(2.10) into (2.11) we obtain the condition for the propagation angle ϕ as

$$\tan\left(kn_1 a \sin\phi - \frac{m\pi}{2}\right) = \sqrt{\frac{2\Delta}{\sin^2\phi} - 1} \tag{2.12}$$

Equation (2.12) shows that the propagation angle of a light ray is discrete and is determined by the waveguide structure (core radius a, refractive index n_1, refractive index deference Δ) and the wavelength λ of the light source (wavenumber is $k = \frac{2\pi}{\lambda}$) [?]. The optical field distribution that satisfies the phase matching condition of (2.12) is called *mode*. The allowed value of propagation constant β of (2.5) is also discrete and is denoted as an eigenvalue. The mode that has the minimum angle ϕ in Eq. (2.12) (m=0) is the fundamental mode; the other modes, having larger angles, are higher order modes ($m \geq 1$).

Fig. 2.4 schematically shows the formation of modes (standing waves) for (a) the fundamental mode and (b) a higher order mode, respectively, through the interference of light waves. In the figure, the solid line represents a positive phase front and a dotted line represents a negative phase front, respectively. The electric field amplitude becomes the maximum (minimum) at the point where two positive (negative) phase fronts interfere. In contrast, the electric filed amplitude becomes almost zero near the core-cladding interface, since positive and negative phase front cancel out each other. Therefore, the field distribution along the x-(transverse) direction becomes the standing wave and varies periodically along the z-direction with the period

$$\lambda_p = \left(\frac{\lambda}{n_1}\right) / \cos\phi = 2\pi / \beta \tag{2.13}$$

Since $n_1 \sin\phi = \sin\theta \leq \sqrt{n_1^2 - n_0^2}$ from Fig. 2.1, (2.1) and (2.3) give the propagation angle as $\sin\phi \leq \sqrt{2\Delta}$. When we introduce the parameter

$$\zeta = \frac{\sin\phi}{\sqrt{2\Delta}}$$

which normalized to 1, the phase matching equation (2.12) can be rewritten as

$$kn_1 a\sqrt{2\Delta} = \frac{\cos^{-1}\xi + m\pi/2}{\xi} \tag{2.14}$$

The term on the left hand side of (2.14) is know as the normalized frequency, and it is expressed by

$$v = kn_1 a\sqrt{2\Delta} \tag{2.15}$$

When we used the normalized frequency v, the propagation characteristics of the waveguides can be treated generally (independent of each waveguide structure). The relationship between normalized frequency v and ξ (propagation constant β), Equation (2.14) is called the dispersion equation. Fig. 2.5 shows the dispersion curves of a slab waveguide. The crossing point between $\eta = \left(\cos^{-1}\xi + m\pi/2\right)/\xi$ and $\eta = v$ gives ξ_m for each mode number m, and the propagation constant β_m is obtained from (2.5) and (2.13).

It is known from Fig. 2.5 that only the fundamental mode with m=0 can exist when $v < v_c = \pi/2$, v_c determines the single mode condition of the slab waveguide. In other words, the condition in which higher order modes are cutoff. Therefore, it is called the cutoff $v-$value. When we rewrite the cutoff condition in terms of the wavelength we obtain

$$\lambda_c = \frac{2\pi}{v_c} an_1\sqrt{2\Delta} \tag{2.16}$$

λ_c is called the cutoff (free space) wavelength. The waveguide operates in a single mode for wavelengths longer than λ_c. For example, $\lambda_c = 0.8\mu m$ when the core width $2a$=3.54 μm for the slab waveguide of n_1 = 1.46, Δ=0.3% (n_0=1.455).

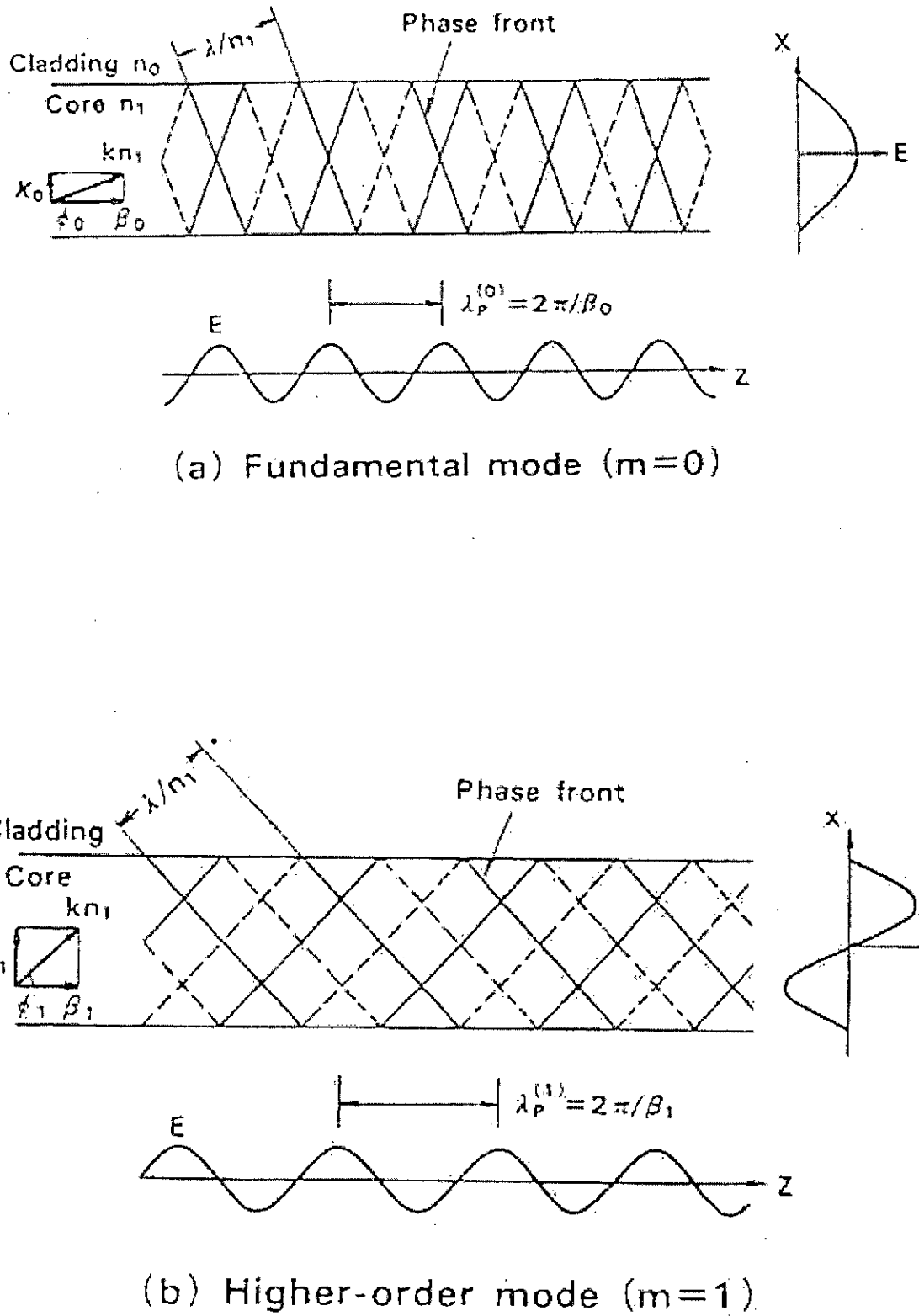

Fig. 2.4: Formation of modes (a) Fundamental mode. (b) Higher order mode.

2.3 MAXWELL'S EQUATIONS

Maxwell's equations in a homogeneous and lossless dielectric medium are written in terms of the electric field **e** and magnetic field **h** as [1], [6]

$$\nabla \times \mathbf{e} = -\mu \frac{\partial \mathbf{h}}{\partial t} \tag{2.17}$$

$$\nabla \times \mathbf{h} = \varepsilon \frac{\partial \mathbf{e}}{\partial t} \tag{2.18}$$

where ε and μ denote the permittivity and permeability of the medium, respectively. ε and μ are related to their respective values in a vacuum of $\varepsilon_0 = 8.854 \times 10^{-12}$ [F/m] and $\mu_0 = 4\pi \times 10^{-7}$ [H/m] by

$$\varepsilon = \varepsilon_0 n^2 \tag{2.19a}$$

$$\mu = \mu_0 \tag{2.19b}$$

where n is the refractive index. The wavenumber of light in the medium is then expressed as [6]

$$\Gamma = \omega\sqrt{\varepsilon\mu} = \omega n\sqrt{\varepsilon_0\mu_0} = kn \tag{2.20}$$

In (2.20), ω is an angular frequency of the sinusoidally varying electromagnetic fields with respect to time; k is the wavenumber in a vacuum, which is related to the angular frequency ω by

$$k = \omega\sqrt{\varepsilon_0\mu_0} = \frac{\omega}{c} \tag{2.20}$$

In (2.21), c is the velocity of light in a vacuum, given by

$$c = \frac{1}{\sqrt{\varepsilon_0\mu_0}} = 2.998 \times 10^8 \text{ [m/s]} \tag{2.22}$$

The fact that the units for light velocity c are m/s is confirmed from the units of the permittivity ε_0 [F/m] and permeability μ_0 [H/m] as

$$\frac{1}{\sqrt{[\text{F/m}][\text{H/m}]}} = \frac{\text{m}}{\sqrt{\text{F}\cdot\text{H}}} = \frac{\text{m}}{\sqrt{[\text{A}\cdot\text{s/V}][\text{V}\cdot\text{s/A}]}} = \frac{\text{m}}{\text{s}}$$

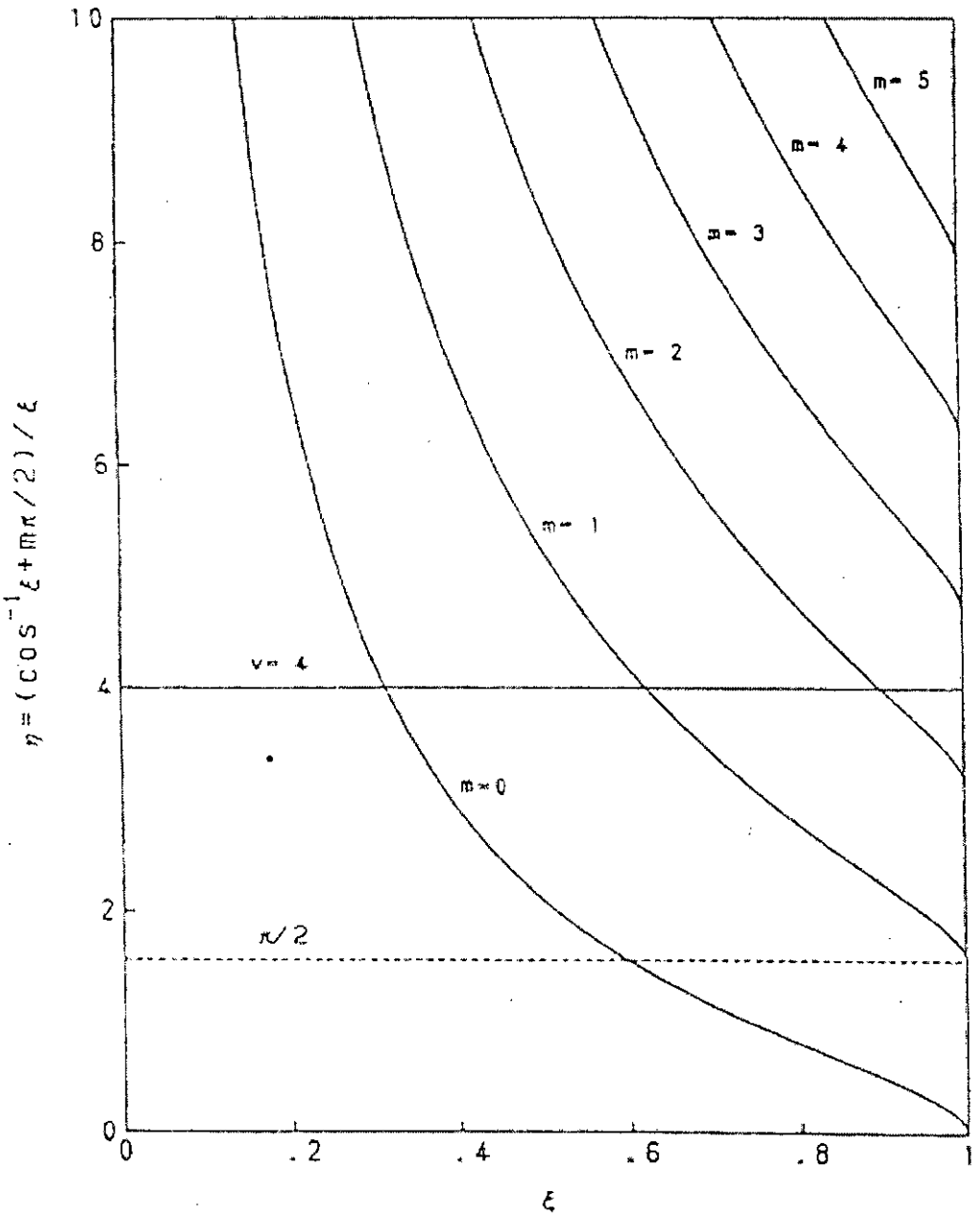

Fig.2.5: Dispersion curves of a slab waveguide.

When the frequency of the electromagnetic wave is f [Hz], it propagates c/f [m] in one period of sinusoidal variation. Then the wavelength of electromagnetic wave is obtained by

$$\lambda = \frac{c}{f} = \frac{\omega / k}{f} = \frac{2\pi}{k} \tag{2.23}$$

where $\omega = 2\pi f$. When the electromagnetic fields $\mathbf{e}$ and $\mathbf{h}$ are sinusoidal functions of time. They are usually represented by complex amplitudes, i.e., the so-called phasors. As an example consider the electric field vector

$$\mathbf{e}(t) = |\mathbf{E}| \cos(\omega t + \phi) \tag{2.24}$$

where $|\mathbf{E}|$ is the amplitude and ϕ is the phase. Defining the complex amplitude of $\mathbf{e}(t)$ by

$$\mathbf{E} = |\mathbf{E}| e^{-j\omega t} \tag{2.25}$$

Eq. (2.24) can be written as

$$\mathbf{e}(t) = \mathrm{Re}\{\mathbf{E} e^{j\omega t}\} \tag{2.26}$$

We will often represent $\mathbf{e}(t)$ by

$$\mathbf{e}(t) = \mathbf{E} e^{j\omega t} \tag{2.27}$$

instead of by (2.24) or (2.26). This expressed is not strictly correct, so when we use this phasor expression we should keep in mind that what is meant by (2.27) is the real part of $\mathbf{E}e^{j\omega t}$. In most mathematical manipulations, such as addition, subtraction, differentiation and integration, the replacement of ((2.26) by the complex form (2.27) poses no problems. However, we should be careful in the manipulations that involve the problems. In these cases we must use the real form of the function (2.24).or complex conjugates.

When we consider an electromagnetic wave having angular frequency ω and the propagating in the z direction with propagation constant β, the electric filed and magnetic field can be expressed as

$$\mathbf{e} = \mathbf{E}(r) e^{j(\omega t - \beta z)} \tag{2.28}$$

$$\mathbf{h} = \mathbf{H}(r) e^{j(\omega t - \beta z)} \tag{2.29}$$

where r denote the position in the plane transverse to the z-axis, Substituting (2.28) and (2.29) into (2.17) and (2.18), the following set of equations are obtained in Cartesian coordinates.

$$\frac{\partial E_z}{\partial y} + j\beta E_y = -j\omega\mu_0 H_x$$

$$-j\beta E_x - \frac{\partial E_z}{\partial x} = -j\omega\mu_0 H_y$$

$$\frac{\partial E_y}{\partial x} - \frac{\partial E_x}{\partial y} = -j\omega\mu_0 H_z$$

$$\frac{\partial H_z}{\partial y} + j\beta H_y = j\omega\varepsilon_0 n^2 E_x \qquad (2.30)$$

$$-j\beta H_x - \frac{\partial H_z}{\partial x} = j\omega\varepsilon_0 n^2 E_y$$

$$\frac{\partial H_y}{\partial x} - \frac{\partial H_x}{\partial y} = -j\omega\varepsilon_0 E_z$$

The foregoing equations are the bases for the analysis of slab and rectangular waveguides. For the analysis of wave propagation in optical fibers, which are axially symmetric, Maxwell's equations are written in terms of cylindrically coordinates:

$$\frac{1}{r}\frac{\partial E_z}{\partial \theta} + j\beta E_\theta = -j\omega\mu_0 H_r$$

$$-j\beta E_r - \frac{\partial E_z}{\partial r} = -j\omega\mu_0 H_\theta$$

$$\frac{1}{r}\frac{\partial}{\partial r}(rE_\theta) - \frac{1}{r}\frac{\partial E_r}{\partial \theta} = -j\omega\mu_0 H_z \qquad (2.31)$$

$$\frac{1}{r}\frac{\partial H_z}{\partial \theta} + j\beta H_\theta = j\omega\varepsilon_0 n^2 E_r$$

$$-j\beta H_r - \frac{\partial H_z}{\partial r} = j\omega\varepsilon_0 n^2 E_\theta$$

$$\frac{1}{r}\frac{\partial}{\partial r}(rH_\theta) - \frac{1}{r}\frac{\partial H_r}{\partial \theta} = j\omega\varepsilon_0 n^2 E_z$$

Maxwell's equations (2.30) or (2.31) do not determine the electromagnetic field completely out of the infinite possibilities of solutions of Maxwell's equations. We must select those that also satisfy the boundary conditions of the respective problems. The most common type of boundary condition occurs when there are discontinuities in the dielectric constant (refractive index), as shown in Fig. 2.1. At the boundary condition the tangential components of the electric field and magnetic field should satisfy the

conditions

$$E_t^{(1)} = E_t^{(2)} \tag{2.32}$$

$$H_t^{(1)} = H_t^{(2)} \tag{2.33}$$

where the subscript t denotes the tangential components of the boundary and the superscript (1) and (2) indicate the medium, respectively. Equations (2.32) and (2.33) mean that the tangential components of the electromagnetic fields must be continuous at the boundary. There are also natural boundary conditions that require the electromagnetic field to be zero at infinity.

2.4 PROPAGATING POWER

Consider Gauss's theorem for vector A in an arbitrary volume V

$$\iiint_V \nabla \cdot \mathbf{A}\, dv = \iint_S \mathbf{A} \cdot \mathbf{n}\, ds \tag{2.34}$$

where $\mathbf{n}$ is the outward directed unit vector normal to the surface S enclosing V and dv and ds are the differential volume and surface elements, respectively. When we set $\mathbf{A} = \mathbf{e} \times \mathbf{h}$ in (2.23) and use the vector identity

$$\nabla \cdot (\mathbf{e} \times \mathbf{h}) = \mathbf{h} \cdot \nabla \times \mathbf{e} - \mathbf{e} \cdot \nabla \times \mathbf{h} \tag{2.35}$$

We obtain the following equation for electromagnetic fields:

$$\iiint_V (\mathbf{h} \cdot \nabla \times \mathbf{e} - \mathbf{e} \cdot \nabla \times \mathbf{h})\, dv = \iint_S (\mathbf{e} \times \mathbf{h}) \cdot \mathbf{n}\, ds \tag{2.36}$$

Substituting (2.17) and (2.18) into (2.36) results in

$$\iiint_V \left(\varepsilon \mathbf{e} \cdot \frac{\partial \mathbf{e}}{\partial t} + \mu \mathbf{h} \cdot \frac{\partial \mathbf{h}}{\partial t} \right) = -\iint_S (\mathbf{e} \times \mathbf{h}) \cdot \mathbf{n}\, ds \tag{2.37}$$

The first term in (2.37)

$$\varepsilon \mathbf{e} \cdot \frac{\partial \mathbf{e}}{\partial t} = \frac{\partial}{\partial t} \left(\frac{\varepsilon}{2} \mathbf{e} \cdot \mathbf{e} \right) \equiv \frac{\partial W_e}{\partial t} \tag{2.38}$$

represents the rate of increase of the electric stored energy W_e and the second term

$$\mu h \cdot \frac{\partial h}{\partial t} = \frac{\partial}{\partial t} \left(\frac{\mu}{2} h \cdot h \right) \equiv \frac{\partial W_h}{\partial t} \tag{2.39}$$

represents the rate of increase of the magnetic stored energy W_h, respectively. Therefore, the left hand side of (2.37) gives the rate of increase of the electromagnetic stored energy in the whole volume V; in other words, it represents the total power flow into the volume bounded by S. When we replace the outward directed unit vector $\mathbf{n}$ by the inward directed unit vector $\mathbf{u}_z(=-\mathbf{n})$, the total power flowing into the volume through surface S is expressed by

$$P = \iint_S -(\mathbf{e}\times\mathbf{h})\cdot\mathbf{n}\, ds = \iint_S (\mathbf{e}\times\mathbf{h})\cdot\mathbf{u}_z\, ds \tag{2.40}$$

Equation (2.40) means that $\mathbf{e}\times\mathbf{h}$ is the vector representing the power flow, and its normal component to the surface $(\mathbf{e}\times\mathbf{h})\cdot\mathbf{u}_z$ gives the amount the power flowing through unit surface area. Therefore, vector $\mathbf{e}\times\mathbf{h}$ represents the power flow density, and

$$\mathbf{S} = \mathbf{e}\times\mathbf{h} \ [\mathrm{W/m^2}] \tag{2.41}$$

is called Poyinting vector. In the equation, $\mathbf{e}$ and $\mathbf{h}$ denote instantaneous fields as function of time t. Let us obtain the average power flow density in an alternating field. The complex electric and magnetic fields can be expressed by

$$\mathbf{e}(t) = \mathrm{Re}\{\mathbf{E}e^{j\omega t}\} = \frac{1}{2}\{\mathbf{E}e^{j\omega t} + \mathbf{E}^* e^{-j\omega t}\} \tag{2.42a}$$

$$\mathbf{h}(t) = \mathrm{Re}\{\mathbf{H}^{j\omega t}\} = \frac{1}{2}\{\mathbf{H}e^{j\omega t} + \mathbf{H}^* e^{-j\omega t}\} \tag{2.42b}$$

where $*$ denotes the complex conjugate. The time average of the normal component of the Poynting vector is then obtained as

$$\begin{aligned}\langle \mathbf{S}\cdot\mathbf{u}_z\rangle &= \langle(\mathbf{e}\times\mathbf{h})\cdot\mathbf{u}_z\rangle \\ &= \frac{1}{4}\left\langle\left[\left(\mathbf{E}e^{j\omega t} + \mathbf{E}^* e^{-j\omega t}\right)\times\mathbf{H}e^{j\omega t} + \mathbf{H}^* e^{-j\omega t}\right]\cdot\mathbf{u}_z\right\rangle \\ &= \frac{1}{4}\left(\mathbf{E}\times\mathbf{H}^* + \mathbf{E}^*\times\mathbf{H}\right)\cdot\mathbf{u}_z \\ &= \frac{1}{2}\mathrm{Re}\{(\mathbf{E}\times\mathbf{H}^*)\cdot\mathbf{u}_z\}\end{aligned} \tag{2.43}$$

where $\langle\ \rangle$ denotes a time average. Then the time average of the power flow is given by

$$P = \iint_{sd}\frac{1}{2}\mathrm{Re}\{(\mathbf{E}\times\mathbf{H}^*)\cdot\mathbf{u}_z\}\, ds \tag{2.44}$$

Since $\mathbf{E}\times\mathbf{H}^*$ often becomes real in the analysis of optical waveguides, the time average propagation power in (2.44) is expressed by

$$P = \iint_S \frac{1}{2}(\mathbf{E}\times\mathbf{H}*)\cdot\mathbf{u}_z\,ds \tag{2.45}$$

2.5 MODE DESIGNATIONS

The following commonly used mode designations are usually adopted for optical waveguides [1], [6].

- For homogeneous rectangular metallic waveguides

  $TE_{mn}(or\ H_{mn})$ if $(E_Z = 0)$,

  $TM_{mn}(or\ E_{mn})$ if $(H_Z = 0)$.

- For dielectric-slab-loaded rectangular metallic waveguides

  LSE_{mn} if there is no electric field component normal to the slab interface,

  LSM_{mn} if there is no magnetic field component normal to the slab interface.

- For other inhomogeneous waveguides, modes are designated using the dominant transverse component

  E^x_{mn}(or H^y_{mn} or HE_{mn}) if $|E_x| > |E_y|$ (or $|H_y| > |H_x|$),

  E^y_{mn}(or H^x_{mn} or EH_{mn}) if $|E_y| > |E_x|$ (or $|H_x| > |H_y|$).

The indices m and n are used here to designate the number of maxima of the dominant component in the guide region in the x and y direction, respectively.

Chapter 3

FINITE ELEMENT METHOD

In the finite element method (FEM), instead of differential equations (governing equations) for the system under consideration, corresponding functionals (variational expressions) to which a variational principle is applied are set up, where the region of interest is divided into the so-called elements; an equivalent discretized model for each element is constructed; and then all the element contributions to the system are assembled. In other words, the FEM can be constructed a subclass of the Rayleigh-Ritz method, in which piecewise defined polynomial functions are used for trial functions and infinite degrees of freedom of the system are discretized or replaced by a finite number of unknown parameters. In classic analytical procedures without subdivision processes, the system is modeled using analytical functions defined over the whole region of interest, and therefore these procedures generally are applicable only to simple geometries and materials. Of the various forms of discretization possible, one of the simplest is the finite difference method (FDM). And its traditional versions use regular grid; that is, a rectangular grid with nodes at the intersections of orthogonal straight lines. However, a regular grid is not suitable for curved boundaries or interfaces, because they intersect gridlines obliquely at points other than the nodes. Moreover, a regular grid is not suitable for problems with very steep variations of fields. The FEM is somewhat similar to the FDM. In the FEM, the field region is subdivided into elements; that is, into subregions. Elements can have various shapes, such as triangles and rectangles, allowing the use of an irregular grid. Therefore, the FEM is suitable for problems with very steep variations of fields. Furthermore, this approach can be easily adapted to inhomogeneous and anisotropic problems, and it is possible to systematically increase the accuracy of the solutions obtained, as necessary. Furthermore, the finite element scheme can be established not only the variational method but by the Galerkin method, which is a weighted residual method. Therefore, the FEM may be applicable to problems where

variational principle does not exist or cannot be identified. In this chapter the concept of the FEM and its fundamentals are discussed.

3.1 THE RANGE OF APPLICATIONS

Recently, the finite-element method has been applied to a wide range of problems in electrical and electronic engineering, and many successful results have been obtained as well in the field of electromagnetic-wave engineering, dealing with wave fields. In particular, as the computer becomes faster, it is spawning a new interdisciplinary field, called computational mechanics, in which finite element method plays important roles. The research on the application of the finite-element method to the electromagnetic-wave engineering has been made in earnest since the latter half of the 1960s, particularly from the 1960s, and is now being made extensively. From various viewpoints, electromagnetic wave problems may be classified into the following categories [3]-[4], [8]:

1. steady and unsteady problems
2. eigenvalue and deterministic problems
3. one, two and three dimensional problems
4. scalar and vector field problems
5. homogeneous and inhomogeneous problems
6. isotropic and anisotropic problems
7. conservative and non conservative problems
8. bounded and unbounded field problems
9. linear and non linear problems
10. forward and inverse problems

Depending on the type of problems different boundary value equations arise in the mathematical modeling of physical systems and their solution has long been a major topic in mathematical physics. It is, of course, desirable to solve boundary value problems analytically whenever possible. However, this is generally the exception since an analytical solution can be obtained in only a few cases. In electromagnetics these include the static potential between infinite parallel plates; wave propagation in rectangular, circular, and elliptic waveguides; wave scattering by infinite planes, circular cylinders, spheres etc. Many other problems of practical importance in the engineering fields do not

have an analytical solution. To overcome this difficulty, various approximate methods have been developed, and among them the Ritz and Galerkin methods have been used most widely.

3.2 BASIC STEPS OF THE FINITE ELEMENT METHOD

The finite element method (FEM) is a powerful and versatile tool for solving accurately and efficiently complicated problems [3]-[4]. It is very flexible to handle wide variety of problems without the need for device dependent programming. Its principle characteristic is the discretization of the problem domain into smaller subdomains (or elements) where the mathematical model describing the fields can be simplified. The accuracy of this method depends on these approximations, but also very importantly on the size and distribution of the element divisions throughout the problem domain. The discretization of the domain reduces the problem to an algebraic, matrix form involving large but extremely sparse matrices.

The Finite Element Method (FEM) is a numerical procedure for obtaining solutions to boundary value problems [3]-[4]. The principle of the method is to replace an entire continuous domain by a number of sub-domains in which the unknown function is represented by simple interpolation functions with unknown coefficients. Thus the original boundary value problem with an infinite number of degrees of freedom is converted into a problem with a finite number of degrees of freedoms, or in other words, the solution of the whole system is approximated by a finite number of unknown coefficients. Then a set of algebraic equations or a system of equations is obtained by applying the Ritz variational or Galerkin procedure, and finally, solution of the boundary-value problem is achieved by solving the system of equations. Therefore, a finite element analysis of a boundary value problem should include the following basic steps:

(1) Discretization or subdivision of the domain

(2) Selection of the interpolation functions

(3) Formulation of the system of equations

(4) Solution of the system of equations

3.2.1 DOMAIN DISCRETIZATION

The discretization of the domain, say S, is the first and perhaps the most important step in any finite element analysis because the manner in which the domain is discretized will affect the computer storage requirements, the computation time, and the accuracy of the numerical results. In this step, the entire domain S is subdivided into a number of small domains, denoted as S^e $(e = 1,2,3,.....M)$, with M denoting the total number of sub-domains. These sub-domains are usually referred to as the elements. For one-dimensional domain which is actually a straight or curve line, the elements are often short line segments interconnected to form the original line [Fig. 3.1(a)]. For a two dimensional domain, the elements are usually small triangles and rectangles [Fig. 3.1(b)]. The rectangular elements are best suited for discretizing rectangular regions, while the triangular ones can be used for irregular regions. In a three dimensional solution, the domain may be subdivided into tetrahedra, triangular prism, or rectangular bricks [Fig. 3.1(c)], among which tetrahedra are the simplest and best suited for arbitrary-volume domains. We note that the linear line segments, triangles, and tetrahedra are the basic one, two, and three-dimensional elements.

In most finite element solutions, the problem is formulated in terms of the unknown function ϕ at nodes associated with the elements. For example, a linear line element has two nodes, one at each endpoint. A linear triangular element has three nodes, located at its three vertices, whereas a linear tetrahedron has four nodes, located at its four corners. For implementation it is necessary to describe these nodes. A complete description of a node contains its coordinate values, local number, and global number. The local number of the node indicates its position in the element, whereas the global number specifies its position in the entire system.

The finite element formulation usually results in a banded matrix whose bandwidth is determined by the maximum difference between the global numbers of two nodes in an element. Thus, if a banded matrix solution method is employed to solve the final matrix equation, the computer storage and processing cost can be reduced significantly by

properly numbering the nodes to minimize the bandwidth. However, when bandwidth minimization is unnecessary, the numbering scheme can be arbitrary and is usually chosen to simplify the programming.

The discretization of the domain is usually considered a preprocessing task because it can be completely separated from the other steps. Most well developed finite element program packages have the capability of subdividing an arbitrary shaped line, surface, and volume into the corresponding elements and also provide the optimized global numbering.

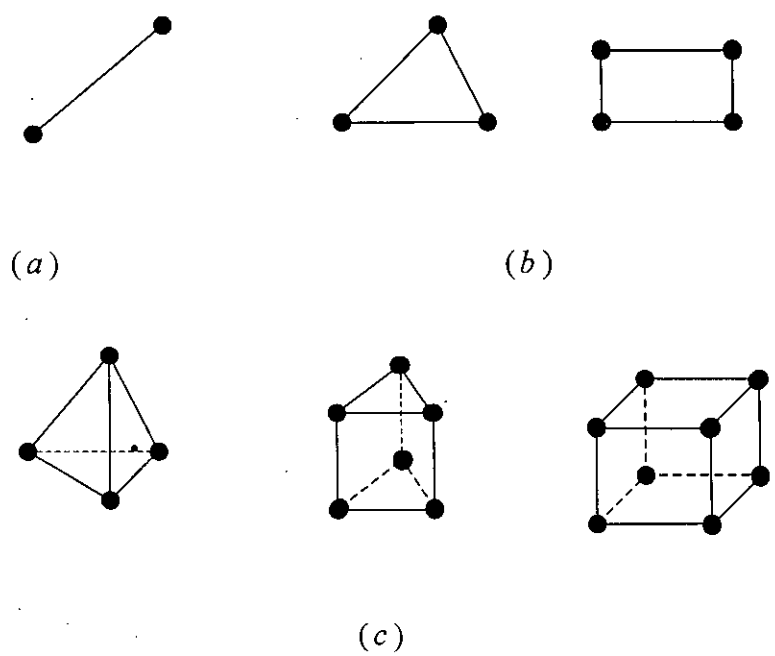

Fig. 3.1 Basic finite elements. (a) One-dimensional. (b) Two-dimensional. (c) Three- dimensional.

3.2.2 SELECTION OF INTERPOLATION FUNCTIONS

The second step of a finite element analysis is to select an interpolation function that provides an approximation of the unknown solution within an element. The interpolation is usually selected to be a polynomial of first (linear), second (quadratic), or higher order.

Higher-order polynomials, although more accurate, usually result in a more complicated formulation. Hence, the simple and basic linear interpolation is still widely used. Once the order of the polynomial is selected, we can drive an expression for the unknown solution in an element, say element e, in the following form:

$$\phi^e = \sum_{j=1}^{n} N_j^e \phi_j^e = \left\{N^e\right\}^T \left\{\phi^e\right\} = \left\{\phi^e\right\}^T \left\{N^e\right\} \tag{3.1}$$

where n is the number of nodes in the element, ϕ_j^e the value of ϕ at node j of the element, and N_j^e the interpolation function, which is also known as expansion or basis function. The highest order of N_j^e is referred to as the order of the element; for example, if N_j^e is a linear function, the element e is a linear element. An important feature of the functions N_j^e is that they are nonzero only within element e, and outside this element they vanish.

3.2.3 FORMULATION OF THE SYSTEM OF EQUATIONS

The third step, also a major step in a finite element analysis, is to formulate the system of equations. To clarify ideas of the FEM, consider a particular problem governed by the Helmholtz equation. The specific governing equation is now written for a domain Ω shown in Fig. 3.2 as

$$\nabla^2\phi + k^2\phi = 0 \quad \text{in } \Omega \tag{3.2}$$

where ϕ is the electric or magnetic field component and the quantity k^2 is a constant related to frequency. The Laplacian operator is given by

$$\nabla^2 = \partial^2/\partial x + \partial^2/\partial y + \partial^2/\partial z \tag{3.3}$$

in Cartesian coordinates.

Now, we assume that the boundary Γ of the region Ω consist of partly of Γ_f on which the value of ϕ is given as $\hat{\phi}$ and partly of Γ_n on which the value of $\partial\phi/\partial n \equiv \psi$ is given by $\hat{\psi}$, namely,

$$\phi = \hat{\phi} \text{ on } \Gamma_f \tag{3.4}$$

$$\partial\phi/\partial n = \mathbf{n}\cdot\nabla\phi = \hat{\psi} \quad \text{on } \Gamma_n \tag{3.5}$$

where **n** is the outward unit normal vector. The gradient operator is described by the matrix-differential operator

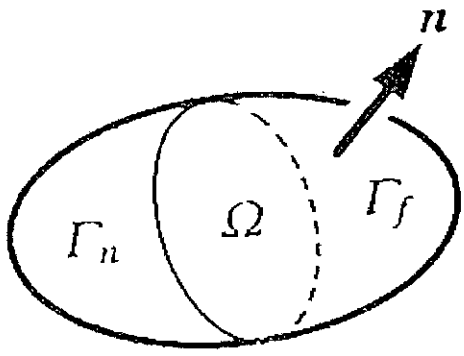

Fig. 3.2 Three dimensional region Ω surrounded by boundaries Γ_f and Γ_n

$$\nabla = \begin{bmatrix} \partial/\partial x \\ \partial/\partial y \\ \partial/\partial z \end{bmatrix} \tag{3.6}$$

in Cartesian coordinates.

The boundary conditions, Esq. (3.4) and (3.5), are called Dirichlet and Neumann boundary conditions, respectively. Considering these boundary conditions, the functional for Eq. (3.2) is given by

$$F = \frac{1}{2}\iiint_{\Omega}\left[(\nabla\phi)^2 - k^2\phi^2\right]d\Omega - \iint_{\Gamma_n}\phi\hat{\psi}\,d\Gamma \tag{3.7}$$

The first and second terms in the right-hand side of Eq. (3.2) denote the integrals over the region Ω and along the boundary Γ_n, respectively. The Euler equation derived by the stationary requirement

$$\partial F = 0 \tag{3.8}$$

coincides with the governing equation, namely Eq. (3.2). The boundary condition in Eq. (3.5) is called the natural boundary condition, because this condition is automatically satisfied in the variational procedure. On the other hand, the boundary condition in Eq.

(3.4) should be imposed on trial functions; therefore, this condition is called the forced boundary condition.

Dividing the region Ω into a number of elements e and considering the functional F_e

$$F_e = \frac{1}{2}\iiint_e \left[(\nabla\phi)^2 - k^2\phi^2\right] d\Omega - \iint_{\Gamma_e} \phi\psi \, d\Gamma \tag{3.9}$$

for each element, the functional for the whole region is given by

$$F = \sum_e F_e \tag{3.10}$$

The first and second terms in the right-hand side of Eq. (3.9) denote the integrals over each element e and along the element boundary Γ_e, respectively, and the summation $\sum_e$ extends over all different elements.

Arranging n nodes in each element, ϕ can be approximated as

$$\phi = \sum_{i=1}^{n} N_i \phi_i \tag{3.11}$$

where ϕ_i is the with nodal parameter of the element e and N_i is the interpolation or shape function.

When the functional value contains first order derivatives, to guarantee the convergence of the solutions, the shape functions N_i should satisfy the following two conditions:

(1) The variable ϕ and its derivatives must include the constant terms.

(2) The variable ϕ must be continuous at the interface between two adjacent elements.

These are called the completeness and compatibility conditions, respectively. The completeness condition is simple to satisfy if complete polynomial expressions are used in each element. First-order or linear elements are the most fundamental ones, and use first-order polynomials. Higher-order elements, on the other hand, use higher-order polynomials. The number of nodes within each element, n, coincides with the number of terms in a complete polynomial expansion, and nodes are arranged to satisfy the compatibility condition.

We can express Eq. (3.11) in matrix form:

$$\phi = \{N\}^T \{\phi\}_e \tag{3.12}$$

where the components of the $\{\phi\}_e$ and $\{N\}$ vectors are ϕ_i and N_i ,respectively, and T, $\{\cdot\}$, and $\{\cdot\}^T$ denote a transpose, a column vector, and row vector, respectively. Substituting Eq. (3.11) into Eq. (3.9), we obtain

$$F_e = \frac{1}{2}\sum_i \sum_j \left[\phi_i \left(K_{ij} - k^2 M_{ij}\right)\phi_j\right] - \sum_i \phi_i \psi_i \tag{3.13}$$

with

$$K_{ij} = \iiint_{\Omega} (\nabla N_i)\cdot(\nabla N_j)\, d\Omega \tag{3.14}$$

$$M_{ij} = \iiint_{\Omega} N_i N_j \, d\Omega \tag{3.15}$$

$$\Psi_i = \iint_{\Gamma} N_i \psi \, d\Gamma \tag{3.16}$$

We can express Eq. (3.13) in matrix form as

$$F_e = \frac{1}{2}\{\phi\}_e^T [K]_e \{\phi\}_e - \frac{1}{2} k^2 \{\phi\}_e^T [M]_e \{\phi\}_e - \{\phi\}_e^T \{\psi\}_e \tag{3.17}$$

where the components of the $[K]_e$ and $[M]_e$ matrices are K_{ij} and M_{ij}, respectively.

Assuming that boundary conditions at the interface between the two adjacent elements are $\phi_1 = \phi_2$ and $\psi_1 = -\psi_2$, the functional for the whole region is given by

$$F = \sum_e F_e = \frac{1}{2}\{\phi\}^T [A]\{\phi\} - \{\phi\}^T \{\psi\} \tag{3.18}$$

with

$$[A] = [K] - k^2 [M] \tag{3.19}$$

where the components of the $\{\phi\}$ vector are the values of ϕ at all nodes, and the global matrices $[K]$ and $[M]$ come from adding the element matrices, $[K]_e$ and $[M]_e$, respectively. The components of the $\{\phi\}$ vector corresponding to nodes on the boundaries Γ_n and Γ_f are $\hat{\psi}$ and unknown, respectively, and the other components become zero. The first variation δF is given by

$$\delta F = \frac{1}{2}\delta\{\phi\}^T[A]\{\phi\} + \frac{1}{2}\{\phi\}^T[A]\delta\{\phi\} - \delta\{\phi\}^T\{\psi\} \tag{3.20}$$

where $\delta\{\phi\}$ is small admissible variation of $\{\phi\}$.

As the matrix $[A]$ is symmetric, we have

$$\delta\{\phi\}^T[A]\{\phi\} = \{\phi\}^T[A]\delta\{\phi\} \tag{3.21}$$

Substituing Eq. (3.21) into Eq. (3.20), δF becomes

$$\delta F = \delta\{\phi\}^T[A]\{\phi\}\{\phi\}^T - \delta\{\phi\}^T\{\psi\} \tag{3.22}$$

Using the variational principle, Eq. (3.8), the discretized algebraic equation is derived as

$$[A]\{\phi\} = \{\psi\} \tag{3.23}$$

For free vibration problems without the excitation term $\{\psi\}$, one obtains

$$[K]\{\phi\} - k^2[M]\{\phi\} = \{0\} \tag{3.24}$$

where $\{0\}$ is a null vector. The so-called eigenvalue problem, Eq. (3.24), can be solved by using computer programs for generalized eigenvalue problems, and thus we obtain eigenvalues for the system under consideration, namely, eigen frequencies.

In this section Eq. (3.23) was derived by applying a variational principle to the functional, Eq. (3.9). It should be noted that the Galerkin method will yield the identical equation to Eq. (3.23) derived from a variational principle. The variational expression, Eq. (3.9), is not suitable for the study of dissipative systems, and the use of the Glarkin procedure is recommended.

Before the system of equations is ready to be solved for a specific solution, we need to apply the required boundary conditions. There are two kinds of boundary conditions that are often encountered: one is the Dirichlet boundary condition, which prescribes ϕ at the boundary, and the other is the homogeneous Neumann boundary condition, which requires the normal derivative of ϕ to vanish at the boundary. The first is an essential boundary condition that must be imposed explicitly, in contrast to the second, which is usually satisfied implicitly and automatically in the solution process. For this reason, the second one is often called the natural boundary condition.

It is seen that in this step we actually have three sub-steps. First, we formulate the elemental equation using either of the two methods. Then, we sum the elemental equations over all elements to form the system of equations and this process is called assembly. Finally, we impose the boundary conditions to obtain the final form of the system of equations. We note that in computer implementation, the three sub-steps are usually not separated; in stead, they are intertwined. The generation of the elemental matrix and the imposition of the boundary conditions usually take place during the process of assembly.

3.2.4 SOLUTION OF THE SYSTEM OF EQUATIONS

Solving the system of equations is the final step in a finite element analysis. The resultant system has one of the following two forms:

$$[K]\{\phi\} = \{b\} \tag{3.26}$$

or

$$[A]\{\phi\} = \lambda[B]\{\phi\} \tag{3.27}$$

- Equation (3.26) is of the deterministic type, resulting from either an inhomogeneous differential equation or inhomogeneous boundary conditions or both.

In electromagnetics, deterministic systems are usually associated with scattering, radiation, and other deterministic problems where there exists a source or excitation. To the contrary, (3.27) is of the eigenvalue type, resulting from a homogeneous governing differential equation and homogeneous boundary conditions. In electromagnetics, eigenvalue systems are usually associated with source free problems such as wave propagation in waveguides and resonance in cavities. In this case, the known vector $\{b\}$ vanishes and the matrix $[K]$ can be written as $[A]-\lambda[B]$, where λ denotes the unknown eigenvalues. Once we have solved the system of equations for $\{\phi\}$, we can then compute the desired parameters, such as capacitance, inductance, input impedance, and scattering or radiation patterns and display the result in form of curves, plots, or color pictures, which are more meaningful interpretable. This final stage, often referred to as post-processing, can also be separated completely from the other steps.

Chapter 4

FINITE ELEMENT FORMULATION WITH HYBRID EDGE/NODAL ELEMENT

For a proper computer simulation of the electromagnetic fields in a dielectric waveguide we have to begin with an adequate mathematical description of the problem. The primary concern of this chapter is the definition of the mathematical model, that is, the interpretation of the physical problem in mathematical terms. This mathematical model of the dielectric waveguide problem will be described in detail in section 4.1. Following this discussion, the details of the hybrid edge/nodal element and it's construction are shown in section 4.2. Next we show the discretization process with this element [26]-[27], [31]-[32], [43] and the analysis procedure of loss by perturbation technique [43].

4.1 DESCRIPTION OF THE PROBLEM

The term dielectric waveguide is used throughout this thesis to describe a waveguide of general cross section as shown in Fig. 4.1. We assume the waveguide to be uniform along the z- axis and with an arbitrary cross section Ω in the plane x-y. The cross section of the guide is bounded by an outer boundary C_0 which can extend (partially or completely) to infinity. The cross section can consist of regions of linear dielectric materials and also perfectly conducting material (imperfect dielectrics and imperfect conductors are represented as dielectric materials with a complex permittivity). In electromagnetic theory, idealizations such as perfect electric conductors (conductors, electrodes or baffles) are frequently adopted. Perfectly conducting materials, such as regions S_1 in the figure, will in practice be considered outside the region of interest because the electromagnetic field will be zero there. The boundaries of all such regions, such as C_1 in the figure, are part of the problem boundary therefore, and boundary conditions are applied on them. Thus in the configuration shown in Fig. 4.1 the total boundary C is composed of C_0 and C_1

(and of the boundaries of any other region likes S_1). It is convenient to introduce some abbreviated notation for this and we adopt the point set union descriptor $\cup$ for the union of multiple point sets giving $C = C_0 \cup C_1$. This set theory language for "C is the set of all points of the outer boundary point set C_0 and point set C_1".

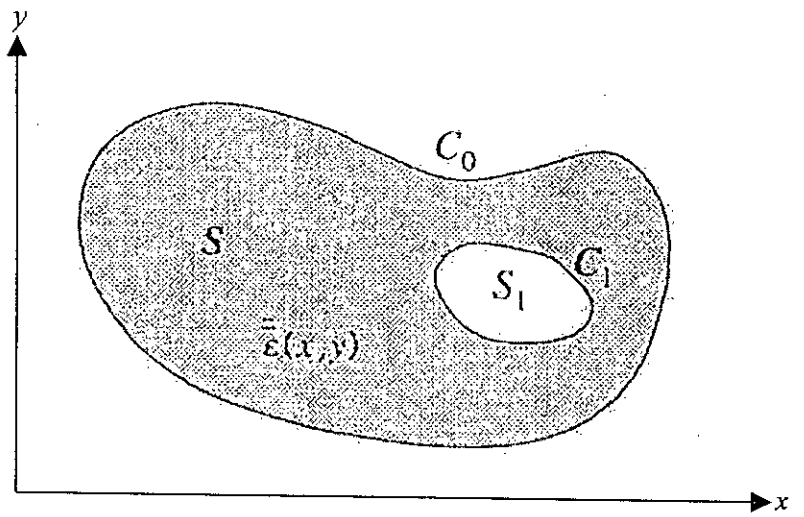

Fig. 4.1: A general structure of the dielectric waveguide.

The complete region of interest then consists of S and its boundary C. The closed region (including its boundary) is denoted by $\bar{S}$. The dielectric material in $\bar{S}$ can be arbitrary inhomogeneous, anisotropic and dissipative or active (material showing uniform gain along z can be represented in this model by a positive value of the imaginary part of the permittivity, or a negative conductivity) and the complete structure can be bounded or unbounded. Roughly, a closed region is one that includes its boundary and a boundary region is one that does not extended to infinity. We assume that C, the boundary of $\bar{S}$, consists of any combination of the following three types: perfect electric conductors, perfect magnetic walls or regions extending to infinity. Perfect electric and magnetic walls can appear in any type of waveguide in microwave and optics when considerations are used to divide and reduce the region of study.

We, in general consider the material anisotropic having diagonal permittivity tensor and diagonal permeability tensor, such that

$$[\varepsilon]=\begin{bmatrix}\varepsilon_{xx} & 0 & 0\\ 0 & \varepsilon_{yy} & 0\\ 0 & 0 & \varepsilon_{zz}\end{bmatrix}$$

$$[\mu]=\begin{bmatrix}\mu_{xx} & 0 & 0\\ 0 & \mu_{yy} & 0\\ 0 & 0 & \mu_{zz}\end{bmatrix}$$

The most direct approach is based on a full electric and magnetic field description of the problem. Assuming a harmonic time dependence of the form $\exp(j\omega t)$, where ω is the real angular frequency, the governing source free Maxwell's equations are

$$\nabla\times\mathbf{E}=-j\omega\,\mathbf{B}=-j\omega\mu_0[\mu]\cdot\mathbf{H} \tag{4.1}$$

$$\nabla\times\mathbf{H}=-j\omega\,\mathbf{D}=-j\omega\varepsilon_0[\varepsilon]\cdot\mathbf{E} \tag{4.2}$$

$$\nabla\cdot\mathbf{D}=\nabla\cdot(\varepsilon_0[\varepsilon]\cdot\mathbf{E})=0 \tag{4.3}$$

$$\nabla\cdot\mathbf{B}=\nabla\cdot(\mu_0[\mu]\cdot\mathbf{H})=0 \tag{4.4}$$

where **E** and **H** are the electric and magnetic field, respectively, **D** and **B** are the electric flux and magnetic flux densities, respectively, $[\varepsilon]$ and $[\mu]$ are the relative permittivity and permeability tensors, and ε_0 and μ_0 are the vacuum permittivity and permeability scalars, respectively. Here, we also assume that the *z*-dependence of the propagation constant β is $\exp(-j\beta z)$, where *z* is the propagation direction. There symbolic equations are frequently displayed in the component form by means of a matrix representation, with fields described by the column matrices

$$\mathbf{E}=\begin{bmatrix}E_x\\ E_y\\ E_z\end{bmatrix},\qquad \mathbf{H}=\begin{bmatrix}H_x\\ H_y\\ H_z\end{bmatrix},\quad \text{etc.}$$

and the curl and divergence operators described by the matrix-differential operators

$$\nabla\times=\begin{bmatrix}0 & -\partial/\partial z & \partial/\partial y\\ \partial/\partial z & 0 & -\partial/\partial x\\ -\partial/\partial y & \partial/\partial x & 0\end{bmatrix}$$

$$\nabla\cdot = \left[\partial/\partial x \quad \partial/\partial y \quad \partial/\partial z \right]$$

in Cartesian coordinates. For field quantities, there are two more constitutive equations

$$\mathbf{D} = \varepsilon_0 [\varepsilon] \mathbf{E}$$

$$\mathbf{B} = \mu_0 [\mu] \mathbf{H}$$

The field vectors **E**, **D**, **H**, **B** should also satisfy the associated boundary conditions. At an abrupt interface between two contiguous media *a* and *b*, the boundary conditions are

$$\mathbf{n} \times (\mathbf{E}_a - \mathbf{E}_b) = 0 \tag{4.5a}$$

$$\mathbf{n} \times (\mathbf{H}_a - \mathbf{H}_b) = 0 \tag{4.5b}$$

$$\mathbf{n} \times (\mathbf{D}_a - \mathbf{D}_b) = \varepsilon_0 \, \mathbf{n} \left([\varepsilon_a] \cdot \mathbf{E}_a - [\varepsilon_b] \cdot \mathbf{E}_b \right) = 0 \tag{4.5c}$$

$$\mathbf{n} \times (\mathbf{B}_a - \mathbf{B}_b) = \mu_0 \, \mathbf{n} \left([\mu_a] \cdot \mathbf{H}_a - [\mu_b] \cdot \mathbf{H}_b \right) = 0 \tag{4.5d}$$

n is normal unit vector at the interface pointing from medium *a* towards medium *b*.

These conditions assume a simplified form at the boundary:

On a perfect electric conductor, the boundary conditions are

$$\mathbf{n} \times \mathbf{E} = 0 \tag{4.5e}$$

$$\mathbf{n} \cdot \mathbf{B} = 0 \quad (\text{or } \mathbf{n} \cdot [\mu] \cdot \mathbf{H} = 0) \tag{4.5f}$$

On a perfect magnetic conductor

$$\mathbf{n} \times \mathbf{H} = 0 \tag{4.5g}$$

$$\mathbf{n} \cdot \mathbf{D} = 0 \quad (\text{or } \mathbf{n} \cdot [\varepsilon] \cdot \mathbf{E} = 0) \tag{4.5h}$$

And at infinity, for all non-radiation waveguide modes, all field components vanish and we can simply consider

$$\mathbf{E} = \mathbf{D} = \mathbf{H} = \mathbf{B} = \mathbf{0} \tag{4.5i}$$

The situation can be effectively treated using infinite elements, as we shall see later, respecting the fields in the region that extends to infinity by simple functions, which satisfy the condition (4.5i) asymptotically at infinity. Leaky waves cannot be treated in this way. The same treatment can be applied to non radiating modes too, for added accuracy, instead of using infinite elements.

For simplicity, we will not consider the condition at infinity in the following discussion. The boundary problem is unambiguously defined by the two curl equations (4.5a) and (4.5b), and either the tangential boundary conditions (4.5a), (4.5b), (4.5e) and (4.5g) or the normal boundary conditions (4.5e), (4.5d), (4.5f) and (4.5h). Solutions to these satisfy implicitly the divergence equations (4.3) and (4.4) and their corresponding complementary boundary conditions. This is evident on taking the divergence of equations (4.1) and (4.2). The boundary value problem can be defined by only one field (i.e., the electric or magnetic field) and the associated boundary conditions. This may simplify the problem and increases the efficiency of a numerical solution by reducing the number of unknowns in the problem. The other field, if necessary, can be obtained later by using then corresponding curl equations (4.1) and (4.2). In this way, the two curl equation (4.1) and (4.2) can be transformed into a single double-curl equation in terms of the magnetic field or electric field only. For example, eliminating the electric field from (4.1) and (4.2) the magnetic field double-curl equation is obtained:

$$\nabla \times \left([\varepsilon]^{-1} \nabla \times \mathbf{H} \right) - k_0^2 [\mu] \mathbf{H} = 0 \tag{4.6}$$

where $k_0 = \omega \sqrt{\mu_0 \varepsilon_0}$ is the free space wave number, $[\varepsilon]$ and $[\mu]$ are relative permittivity and relative permeability tensors, respectively.

The tangential boundary conditions are:

On dielectric interface:

$$\mathbf{n} \times \left(\mathbf{H}_a - \mathbf{H}_b \right) = 0 \tag{4.7a}$$

$$\mathbf{n} \times \left([\varepsilon_a]^{-1} \cdot \nabla \times \mathbf{H}_a - [\varepsilon_b]^{-1} \cdot \nabla \times \mathbf{H}_b \right) = 0 \tag{4.7b}$$

On perfect magnetic walls:

$$\mathbf{n} \times \mathbf{H} = 0 \tag{4.7c}$$

And on perfect electric conditions:

$$\mathbf{n} \times \left([\varepsilon]^{-1} \cdot \nabla \times \mathbf{H} \right) = 0 \tag{4.7d}$$

The normal boundary conditions are:

On dielectric interface:

$$\mathbf{n} \cdot \left([\mu_a] \cdot \mathbf{H}_a - [\mu_b] \cdot \mathbf{H}_b \right) = 0 \tag{4.8a}$$

$$\mathbf{n} \cdot \left(\nabla \times \mathbf{H}_a - \nabla \times \mathbf{H}_b \right) = 0 \tag{4.8b}$$

On perfect electric conditions:

$$\mathbf{n}\cdot[\mu]\cdot\mathbf{H}=0 \tag{4.8c}$$

On perfect magnetic walls:

$$\mathbf{n}\cdot\nabla\cdot\mathbf{H}=0 \tag{4.8d}$$

Similarly one can derive the double-curl electric field equation (from Maxwell's equations) as

$$\nabla\times\left([\mu]^{-1}\nabla\times\mathbf{E}\right)-k_0^2[\varepsilon]\mathbf{E}=0 \tag{4.9}$$

With the corresponding tangential boundary conditions:

On dielectric interface:

$$\mathbf{n}\times\left(\mathbf{E}_a-\mathbf{E}_b\right)=0 \tag{4.10a}$$

$$\mathbf{n}\times\left([\mu_a]^{-1}\cdot\nabla\times\mathbf{E}_a-[\mu_b]^{-1}\cdot\nabla\times\mathbf{E}_b\right)=0 \tag{4.10b}$$

On perfect electric conductors:

$$\mathbf{n}\times\mathbf{E}=0 \tag{4.10c}$$

And on perfect magnetic walls:

$$\mathbf{n}\times([\mu]\cdot\nabla\times\mathbf{E})=0 \tag{4.10d}$$

And the normal boundary conditions:

On dielectric interfaces:

$$\mathbf{n}\cdot\left([\varepsilon_a]\cdot\mathbf{E}_a-[\varepsilon_b]\cdot\mathbf{E}_b\right)=0 \tag{4.11a}$$

$$\mathbf{n}\cdot\left(\nabla\times\mathbf{E}_a-\nabla\times\mathbf{E}_b\right)=0 \tag{4.11b}$$

On perfect magnetic walls:

$$\mathbf{n}\cdot[\varepsilon]\cdot\mathbf{E}=0 \tag{4.11c}$$

And on perfect electric conductors:

$$\mathbf{n}\cdot\nabla\times\mathbf{E}=0 \tag{4.11d}$$

Methods of analyzing truly general anisotropic waveguides, such as the finite element method, usually start either from (4.6) or from (4.9). While the tangential components of the fields are always continuous, the normal components are discontinuous across material interfaces, where jumps in the values of $[\varepsilon]$ and $[\mu]$ occur. However, in nearly

all cases of interest, where $[\mu]=1$, the normal component of magnetic field is also continuous across material interfaces. As far as the enforcement of the boundary conditions are concerned, the use of the full-**H** equation is more convenient. Eventhough, the equations are showing anisotropic form, they can be used for isotropic waveguides with $[\varepsilon]=\varepsilon$ and $[\mu]=1$, where ε is the (scalar) dielectric constant (whose square root is the refractive index).

For the sake of formulation, we express the vector wave equations (4.6), (4.9) as [26]-[27]

$$\nabla\times([p]\nabla\times\varphi)-k_0^2[q]\,\varphi=0 \tag{4.12}$$

with

$$[p]=\begin{bmatrix} p_x & 0 & 0 \\ 0 & p_y & 0 \\ 0 & 0 & p_z \end{bmatrix}$$

$$[q]=\begin{bmatrix} q_x & o & o \\ o & q_y & o \\ o & o & q_z \end{bmatrix}$$

In (4.12), φ denotes either electric field **E** or magnetic field **H**, and the components of $[p]$ and $[q]$ in terms of refractive indices are given by

$$\begin{aligned} p_x &= p_y = p_z = 1 \\ q_x &= n_x^2 \\ q_y &= n_y^2 \\ q_z &= n_z^2 \end{aligned} \qquad \text{for } \varphi=\mathbf{E} \tag{4.13}$$

$$\begin{aligned} p_x &= 1/n_x^2 \\ p_y &= 1/n_y^2 \\ p_z &= 1/n_z^2 \\ q_x &= q_y = q_z = 1 \end{aligned} \qquad \text{for } \varphi=\mathbf{H} \tag{4.14}$$

Here n_x, n_y, n_z are the refractive indices in the x, y, z directions, respectively. The functional for (4.12) which can be obtained by using the variational principle is given by [26]-[27]

$$F=\iint_{\Omega}\left[(\nabla\times\varphi)^*.([p]\nabla\times\varphi)-k_0^2[q]\,\varphi^*.\varphi\right]dx\,dy \tag{4.15}$$

where the asterisk denotes complex conjugate.

4.2 HYBRID EDGE/NODAL ELEMENTS

Various elements are available in the FEM. Also, various special elements are being developed to solve different microwave and optical problems. The hybrid type edge/nodal triangular as well as rectangular elements are such special elements, and have found a great deal of practical applications. In this work, we will use triangular type hybrid element which is composed of edge and nodal elements, where edge elements model the transverse field ensuring tangential continuity along the element interfaces and nodal elements model the axial fields. As the edge elements assign the degrees of freedom to the edges, they allow the field to change its direction abruptly and thus are capable of modeling the field properly at sharp edges at which singularity occurs. With hybrid elements, the finite element method overcomes all the shortcomings, that clouded many of the analyses before.

The hybrid edge/nodal triangular element [26]-[27] for which we will show the formulation is shown in Fig. 4.1. Here the lowest order element is composed of a constant edge element with three tangential unknowns, ϕ_{t1} to ϕ_{t3}, and a linear nodal (conventional Lagrange) element with three axial unknowns, ϕ_{z1} to ϕ_{z3}. The higher order element here is composed of a linear edge element with six tangential unknowns defined at the three vertices of the triangle, ϕ_{t1} to ϕ_{t6}, and a quadratic nodal (conventional Lagrange) element with six axial unknowns, ϕ_{z1} to ϕ_{z6}. For the lowest order element, the tangential component ϕ_t is constant along each side of the triangle, but for higher order element it is approximated to linear order. Since both ϕ_t and ϕ_z are tangential to material interfaces, the tangential continuity can be straightforwardly imposed in the hybrid edge/nodal element analysis.

For the hybrid type edge/nodal triangular element as shown in Fig. 4.1, the transverse components ϕ_x, ϕ_y and the axial component ϕ_z of the unknown $\boldsymbol{\varphi}$ in each element are approximated as

$$\boldsymbol{\varphi} = \begin{bmatrix} \phi_x \\ \phi_y \\ \phi_z \end{bmatrix} = \begin{bmatrix} \{U\}^T \{\phi_t\}_e \\ \{V\}^T \{\phi_t\}_e \\ j\beta \{N\}^T \{\phi_z\}_e \end{bmatrix} \tag{4.16}$$

where $\{\phi_t\}_e$ is the edge variables (field vectors) in the transverse plane for each element, $\{\phi_z\}_e$ is the nodal variables (field vectors) for each element, and T denotes a transpose. Here for the lowest order element of Fig. 4.1(c)

$$\{\phi_t\}_e = [\phi_{t1} \quad \phi_{t2} \quad \phi_{t3}]^T \tag{4.17a}$$

$$\{\phi_z\}_e = [\phi_{z1} \quad \phi_{z2} \quad \phi_{z3}]^T \tag{4.17b}$$

and for the higher order element of Fig. 4.1(f)

$$\{\phi_t\}_e = [\phi_{t1} \quad \phi_{t2} \quad \phi_{t3} \quad \phi_{t4} \quad \phi_{t5} \quad \phi_{t6}]^T \tag{4.18a}$$

$$\{\phi_z\}_e = [\phi_{z1} \quad \phi_{z2} \quad \phi_{z3} \quad \phi_{z4} \quad \phi_{z5} \quad \phi_{z6}]^T \tag{4.18a}$$

Here $\{U\}$ and $\{V\}$ are the shape function vectors for edge elements and $\{N\}$ is the ordinary shape function vector for nodal elements. The shape function vectors are given in Table 4.1 and Table 4.2, where L_k's (k=1,2,3) are the area coordinates, A_e the area of the element, l_k the length of the side between two corner points (x_k, y_k) and (x_l, y_l), and coefficients a_k, b_k, c_l are given by

$$\begin{bmatrix} L_1 \\ L_2 \\ L_3 \end{bmatrix} = \frac{1}{2A_e} \begin{bmatrix} a_1 & b_1 & c_1 \\ a_2 & b_2 & c_2 \\ a_3 & b_3 & c_3 \end{bmatrix} \begin{bmatrix} 1 \\ x \\ y \end{bmatrix} \tag{4.19}$$

with

$$2A_e = \begin{vmatrix} 1 & 1 & 1 \\ x_1 & x_2 & x_3 \\ y_1 & y_2 & y_3 \end{vmatrix} \quad \text{and} \quad \begin{aligned} a_k &= x_l y_m - x_m y_l \\ b_k &= y_l - y_m \\ c_k &= x_m - x_l \end{aligned} \tag{4.20}$$

Here x_k, y_k are the Cartesian coordinates of the corner points 1 to 3 of the triangle, and the subscripts k, l, m always progress modulo 3, that is, cyclically around the vertices of the triangle.

The shape function vectors for the constant edge elements shown in Table 4.1 are very simple compared with the shape functions of other special elements. Noting that the unit tangential vector on the side between two corner points (x_k, y_k) and (x_l, y_l), $\mathbf{t}_k$, is given by

$$\mathbf{t}_k = (c_m / l_k)\,\mathbf{i}_x - (b_m / l_k)\,\mathbf{i}_y \tag{4.21}$$

with $\mathbf{i}_x, \mathbf{i}_y$ being the unit vectors in the x, y directions, respectively. It is seen that for the constant edge elements, the following relations are satisfied:

$$\phi_{tk} = (\phi_{xk}\,\mathbf{i}_x + \phi_{yk}\,\mathbf{i}_y)\,.\,\mathbf{t}_k \tag{4.22}$$

where $\phi_{xk}, \phi_{yk}\,(k = 1,2,3)$ are the values of ϕ_x, ϕ_y at any point on the side of length l_k, respectively, and thus the tangential component ϕ_t is constant along each side of the triangle. The vector shape function for the constant edge element can also be expressed as:

$$\mathbf{W}_k = \mathbf{i}_x U_k + \mathbf{i}_y V_k = (L_i \nabla L_j - L_j \nabla L_i) l_k \tag{4.23}$$

where $\mathbf{W}_k$ is the vector shape function and l_k is the length of kth edge along the node i to node j. For the linear edge elements on the other hand, the following relations are satisfied:

$$\begin{aligned}
\phi_{t1} &= (\phi_{x1}\mathbf{i}_x + \phi_{y1}\mathbf{i}_y).\mathbf{t}_1 \\
\phi_{t2} &= (\phi_{x2}\mathbf{i}_x + \phi_{y2}\mathbf{i}_y).\mathbf{t}_2 \\
\phi_{t3} &= (\phi_{x3}\mathbf{i}_x + \phi_{y3}\mathbf{i}_y).\mathbf{t}_3 \\
\phi_{t4} &= (\phi_{x2}\mathbf{i}_x + \phi_{y2}\mathbf{i}_y).\mathbf{t}_1 \\
\phi_{t5} &= (\phi_{x3}\mathbf{i}_x + \phi_{y3}\mathbf{i}_y).\mathbf{t}_2 \\
\phi_{t6} &= (\phi_{x1}\mathbf{i}_x + \phi_{y1}\mathbf{i}_y).\mathbf{t}_3
\end{aligned} \tag{4.24}$$

where $\phi_{xk}, \phi_{yk}\,(k = 1,2,3)$ are the values of ϕ_x, ϕ_y at the vertices of the triangle, respectively. For better understanding of the shape functions, first we describe the significance of shape functions for a linear nodal triangular element of Fig. 4.2(a). For this element, the shape functions can be derived as

$$N_j^e(x,y) = L_j^e = \frac{1}{2A_e}\left(a_j^e + b_j^e + c_j^e\right)\ (\mathrm{j}=1,\,2,\,3\,) \tag{4.25}$$

It can be easily shown that the shape functions have the property

$$N_j^e\left(x_j^e, y_j^e\right) = \delta_{ij} = \begin{cases} 1 & i=j \\ 0 & i \neq j \end{cases} \tag{4.26}$$

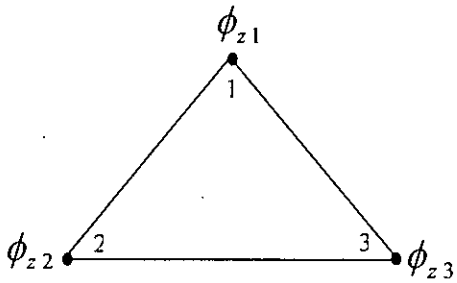

(a) Linear nodal element.

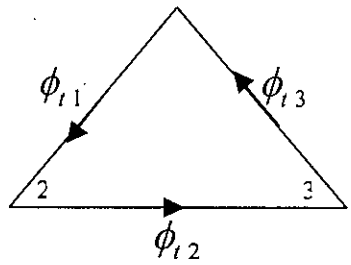

(b) Constant edge element.

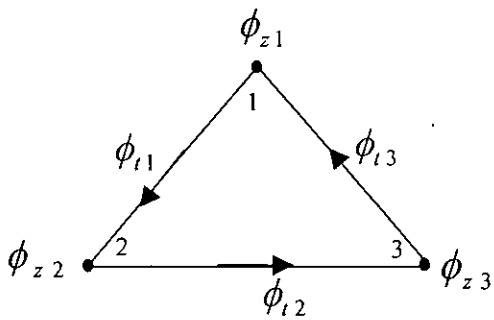

(c) Lowest order hybrid edge/nodal triangular element.

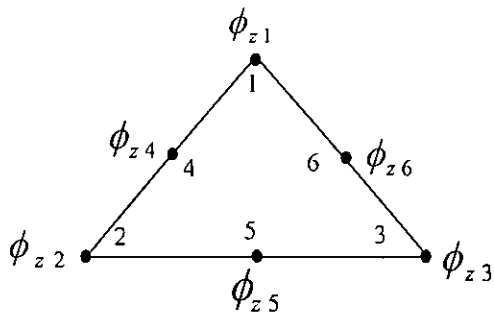

(d) Quadratic nodal element.

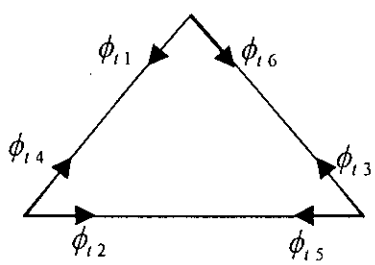

(e) Linear edge element.

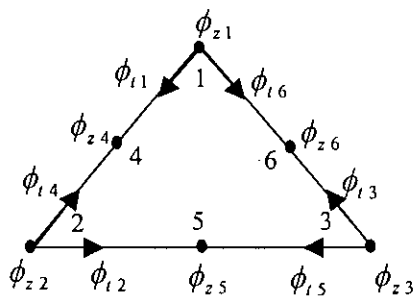

(f) Higher order edge/nodal triangular element.

Fig. 4.2: Hybrid edge/nodal triangular element.

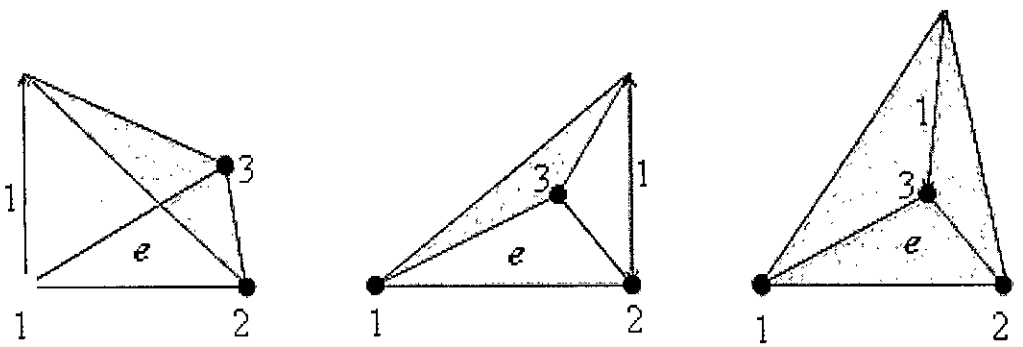

(a) (b) (c)

Fig. 4.3: Shape functions for a linear nodal triangular element. The planer surfaces of the functions are shaded. (a) N_1^e. (b) N_2^e. (c) N_3^e.

and, as a result, at any node, the elemental values ϕ^e reduce to its nodal value ϕ_i^e. Another important feature of $N_j^e(x, y)$ is that it vanishes when the observation point (x, y) is on the element side opposite to the jth node. Therefore, the element value ϕ^e at an element side is not related to the value of ϕ at the opposite side, but rather it is determined by the values at the two endpoints of its associated side. This important feature guarantees the continuity of the solution across the element side. In order to emphasize there features, we show the shape function N_j^e in Fig. 4.3. In Fig. 4.4, we show the vector shape functions as defined by (4.23) for a constant edge triangular element. A vector shape function has a tangential component only at associated edge as shown in Fig. 4.4.

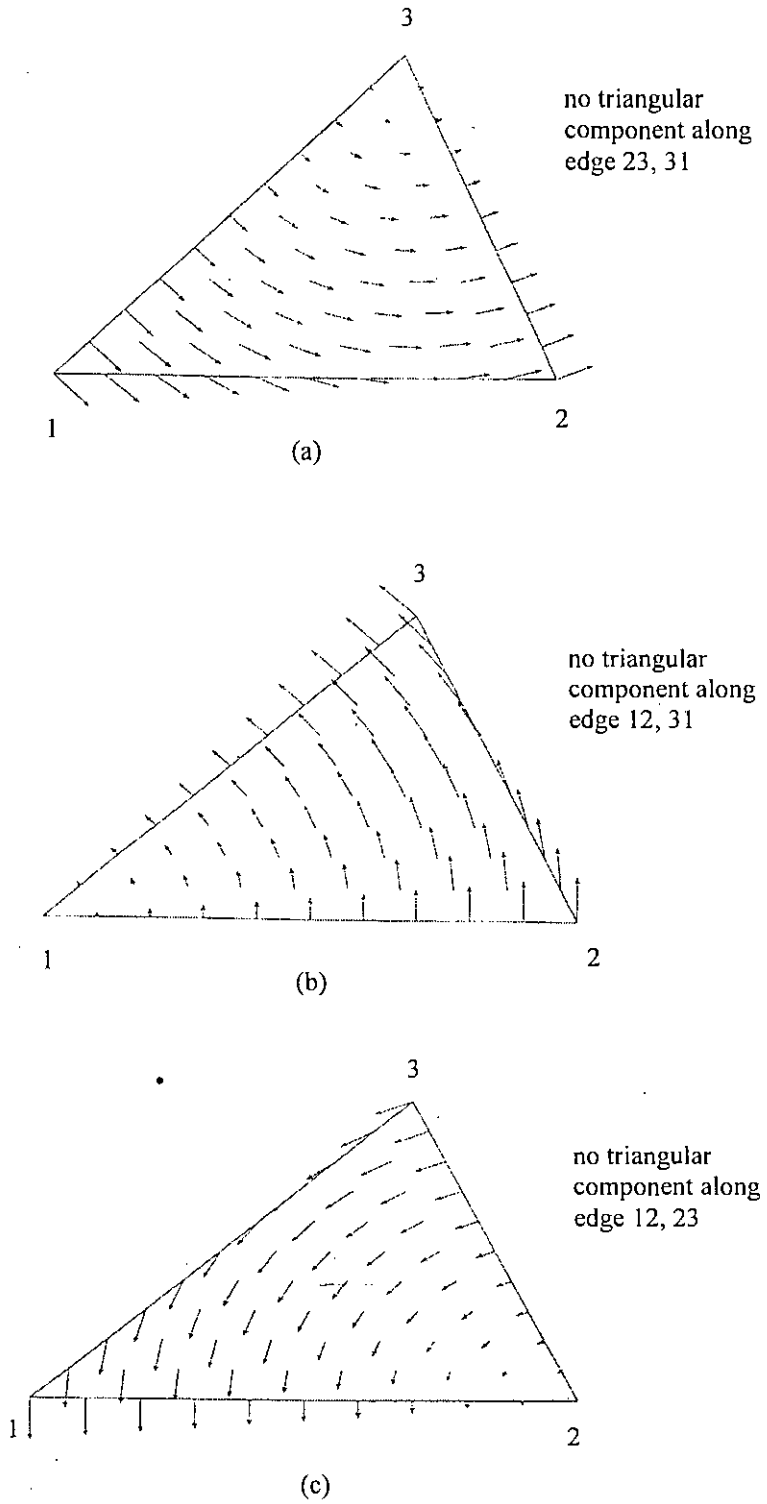

Fig. 4.4: Vector basis functions for a triangular element. (a) $\mathbf{W}_1^e$. (b) $\mathbf{W}_2^e$. (c) $\mathbf{W}_3^e$

TABLE 4.1

Shape function vectors for constant edge and linear nodal element.

$\{U\}$	$\{V\}$	$\{N\}$
$\frac{1}{2A_e}\begin{bmatrix} l_1(y_3-y) \\ l_2(y_1-y) \\ l_3(y_2-y) \end{bmatrix}$	$\frac{1}{2A_e}\begin{bmatrix} l_1(x-x_3) \\ l_2(x-x_1) \\ l_3(x-x_2) \end{bmatrix}$	$\begin{bmatrix} L_1 \\ L_2 \\ L_3 \end{bmatrix}$

TABLE 4.2

Shape function vector for linear edge and quadratic nodal element.

$\{U\}$	$\{V\}$	$\{N\}$
$\frac{1}{2A_e}\begin{bmatrix} l_1b_2L_1 \\ l_2b_3L_2 \\ l_3b_1L_3 \\ -l_1b_1L_2 \\ -l_2b_2L_3 \\ -l_3b_3L_1 \end{bmatrix}$	$\frac{1}{2A_e}\begin{bmatrix} l_1c_2L_1 \\ l_2c_3L_2 \\ l_3c_1L_3 \\ -l_1c_1L_2 \\ -l_2c_2L_3 \\ -l_3c_3L_1 \end{bmatrix}$	$\begin{bmatrix} L_1(2L_1-1) \\ L_2(2L_2-1) \\ L_3(2L_3-1) \\ 4L_1L_2 \\ 4L_2L_3 \\ 4L_3L_1 \end{bmatrix}$

4.3 FINITE ELEMENT DISCRETIZATION

Dividing the waveguide cross section Ω into a number of hybrid type edge/nodal triangular elements shown in Fig. 4.1, we expand the field components in each element using (4.16). Equation (4.16) may be expressed as

$$\boldsymbol{\varphi} = [N]^T \{\phi\}_e \tag{4.27}$$

and then we can express $\nabla \times \boldsymbol{\varphi} = [B]^T \{\phi\}_e$

where
$$[N] = \begin{bmatrix} \{U\} & \{V\} & \{0\} \\ \{0\} & \{0\} & j\beta\{N\} \end{bmatrix}$$

$$[B] = \begin{bmatrix} j\beta\{V\} & -j\beta\{U\} & -\{U_y\} + \{V_x\} \\ j\beta\{N_y\} & -j\beta\{N_x\} & \{0\} \end{bmatrix}$$

and
$$\{\phi\}_e = \begin{bmatrix} \{\phi_t\}_e \\ \{\phi_z\}_e \end{bmatrix}.$$

Here $\{0\}$ is a null vector. We substitute (4.27) into (4.15) and using the standard finite element procedure, we find an eigenvalue equation

$$[K]\{\phi\} - k_o^2 [M]\{\phi\} = \{0\} \tag{4.28}$$

with
$$[K] = \sum_e \iint_e [B]^* \, p [B]^T \, dx\, dy$$
$$[M] = \sum_e \iint_e [N]^* \, q [N]^T \, dx dy$$

and $\{\phi\}$ is the global field vector.

Now equation (4.22) may be rewritten as

$$[K_{tt}]\{\phi_t\} - \beta^2 [K_{tz}]\{\phi_z\} - \beta^2 [M_{tt}]\{\phi_t\} = \{0\}$$
$$-\beta [K_{zt}]\{\phi_t\} + \beta [K_{zz}]\{\phi_z\} = \{0\}$$

So, finally we get

$$\begin{bmatrix} [K_{tt}] & [0] \\ [0] & [0] \end{bmatrix} \begin{bmatrix} \{\phi_t\} \\ \{\phi_z\} \end{bmatrix} - \beta^2 \begin{bmatrix} [M_{tt}] & [K_{tz}] \\ [K_{zt}] & [K_{zz}] \end{bmatrix} \begin{bmatrix} \{\phi_t\} \\ \{\phi_z\} \end{bmatrix} = \{0\}$$

with

$$[K_{tt}] = \sum_e \iint_e [q_x k_0^2 \{U\}\{U\}^T + q_y k_0^2 \{V\}\{V\}^T - p_z \{U_y\}\{U_y\}^T - p_z \{V_x\}\{V_x\}^T$$
$$+ p_z \{U_y\}\{V_x\}^T + p_z \{V_x\}\{U_y\}^T] dx dy$$

$$[K_{tz}] = [K_{zt}]^T = \sum_e \iint_e [p_y \{U\}\{N_x\}^T + p_x \{V\}\{N_y\}^T]\, dxdy$$

$$[K_{zz}] = \sum_e \iint_e [q_z k_0^2 \{N\}\{N\}^T - p_y \{N_x\}\{N_x\}^T - p_x \{N_y\}\{N_y\}^T]\, dxdy$$

$$[M_{tt}] = \sum_e \iint_e [p_y \{U\}\{U\}^T + p_x \{V\}\{V\}^T]\, dxdy$$

The resultant matrix eigenvalue equation thus shows the forms of

$$[K]\{\phi\} - \beta^2 [M]\{\phi\} = \{0\} \tag{4.29}$$

where $\{0\}$ is a null vector, $\{\phi\}$ vector is composed of edge, $\{\phi_t\}$ and nodal, $\{\phi_z\}$ variables, $[K]$ and $[M]$ are finite element matrices and take the form of

$$[K] = \begin{bmatrix} [K_{tt}] & [0] \\ [0] & [0] \end{bmatrix} \quad \text{and} \quad [M] = \begin{bmatrix} [M_{tt}] & [K_{tz}] \\ [K_{zt}] & [K_{zz}] \end{bmatrix}$$

The final eigenvalue problem gives a solution directly for the propagation constant β and the corresponding field distribution and involves the edge and nodal variables. As we used the recent trend of variable transformation [35] in (4.16), it is now possible to exploit sparsity of final matrices, and the method can be applied to analyzing propagation characteristics of integrated waveguides with sharp metal or dielectric edges.

For all the above equations, subscripts *t* and *z* stand for tangential and axial components, respectively. $\{U_y\} \equiv \partial\{U\}/\partial y$, $\{V_x\} \equiv \partial\{V\}/\partial x$, $\{N_x\} \equiv \partial\{N\}/\partial x$, and $\{N_y\} \equiv \partial\{N\}/\partial y$, and their explicit forms are given in Table 4.3 and 4.4. Using equations (4.19) to (4.28), we can easily construct the above matrices for constructing the final global matrix of the eigenvalue problem. The integrals necessary to construct the element matrices are shown in Appendix A and B. In this approach, the frequency is specified as the input parameter and the system is solved for the propagation constant as an eigenvalue. Therefore, it is possible to handle lossy waveguides also. Taking advantages of the sparsity of the finite element matrices in the hybrid element algorithm, it is possible to handle problems involving matrices in several thousands. A detailed formulation is however is given in [27]. For graded index profiles, it is not possible to integrate the expressions for element matrices in closed form as described in appendix A and B. Then numerical integration

has to be used. The Hammer's formula for numerical integration over a triangular element is described in Appendix C.

4.4 CALCULATION OF LOSS BY PERTURBATION METHOD

The perturbation method described in [46] is incorporated with scalar FEM by Themistos et. al. [41]-[42]. We can also use the technique [46] with the edge/nodal element based vector FEM. The attenuation constant due to dielectric loss, α_d, is defined by

$$\alpha_d = \frac{P_d}{2P_0} \tag{4.30}$$

where P_d is the time averaged power dissipated in the dielectric medium and P_0 is the unperturbed power along the direction of propagation and are given by

$$P_d = \omega\,\varepsilon \tan\delta \int_{\Omega} |\mathbf{E}_0|^2 \, d\Omega \tag{4.31}$$

and

$$P_0 = \frac{1}{2}\Re \int_{\Omega} \left(\mathbf{E}_0 \times \mathbf{H}_0^*\right).\hat{\mathbf{z}}\, d\Omega \tag{4.32}$$

where $\mathbf{E}_0$ and $\mathbf{H}_0$ are unperturbed fields of the loss less optical waveguides and $\tan\delta$ is the loss tangent related to the real and imaginary parts of permittivity, $\varepsilon = \varepsilon_r + j\varepsilon_i$ by

$$\tan\delta = \frac{\varepsilon_i}{\varepsilon_r} \tag{4.33}$$

Using Maxwell's equations the power flow P_0 can be expressed in terms of magnetic fields as

$$P_0 = \frac{1}{2}\Re\left\{\int_{\Omega}\left[\left(\frac{1}{j\omega\varepsilon}\nabla\times\mathbf{H}\right)\times\mathbf{H}^*\right]\cdot\mathbf{z}\, d\Omega\right\} \tag{4.34}$$

The hybrid edge/nodal triangular element based finite element procedure is then used over the cross section of the waveguide to calculate unperturbed power flow P_0 and an equation is obtained as

$$P_0 = \{H_t\}^T [C]\{H_t\} \tag{4.35}$$

and to calculate power dissipation in dielectric, an equation is derived as

$$P_d = [\{H_t\}^T [S]\{H_t\} + \{H_z\}^T [T]\{H_z\}] \tag{4.36}$$

where $\{H_t\}$ and $\{H_z\}$ are found from unperturbed field solutions in the form of eigenvectors of the global system. The matrices $[C]$, $[S]$, and $[T]$ can be easily constructed from the finite element matrices and shape function vectors. The τ in the equation denotes a complex conjugate and transpose.

TABLE 4.3

Derivatives of shape functions of lowest order element.

Elements	$\{U_Y\}$	$\{V_x\}$	$\{N_x\}$	$\{N_y\}$
Constant edge and linear nodal elements	$\frac{1}{2A_e}\begin{bmatrix}-l_1\\-l_2\\-l_3\end{bmatrix}$	$\frac{1}{2A_e}\begin{bmatrix}l_1\\l_2\\l_3\end{bmatrix}$	$\frac{1}{2A_e}\begin{bmatrix}b_1\\b_2\\b_3\end{bmatrix}$	$\frac{1}{2A_e}\begin{bmatrix}c_1\\c_2\\c_3\end{bmatrix}$

TABLE 4.4

Derivatives of shape functions of higher order elements.

Element	$\{U_y\}$	$\{V_x\}$	$\{N_x\}$	$\{N_y\}$
Linear edge and quadratic nodal elements	$\frac{1}{4A_e^{\,2}}\begin{bmatrix}l_1b_2c_1\\l_2b_3c_2\\l_3b_1c_3\\-l_1b_1c_2\\-l_2b_2c_3\\-l_3b_3c_1\end{bmatrix}$	$\frac{1}{4A_e^{\,2}}\begin{bmatrix}l_1c_2b_1\\l_2c_3b_1\\l_3c_1b_3\\-l_1c_1b_2\\-l_2c_2b_3\\-l_3c_3b_1\end{bmatrix}$	$\frac{1}{2A_e}\begin{bmatrix}b_1(4L_1-1)\\b_2(4L_2-1)\\b_3(4L_3-1)\\4(b_1L_2+b_2L_1)\\4(b_2L_3+b_3L_2)\\4(b_3L_1+b_1L_3)\end{bmatrix}$	$\frac{1}{2A_e}\begin{bmatrix}c_1(4L_1-1)\\c_2(4L_2-1)\\c_3(4L_3-1)\\4(c_1L_2+c_2L_1)\\4(c_2L_3+c_3L_2)\\4(c_1L_1+c_1L_3)\end{bmatrix}$

Chapter 5

RESULTS AND DISCUSSION

5.1 STRUCTURE OF THE FEM PROGRAM

In the previous chapter, we have described the VFEM formulation for the general waveguide problems. In this chapter, we will demonstrate the capabilities of the finite element approach by applying it to a number of dielectric waveguide structures. The finite element formulation has been programmed with FORTRAN 77 and the system uses some library routines for specific purposes. Before showing numerical results, a brief description of the system should be given.

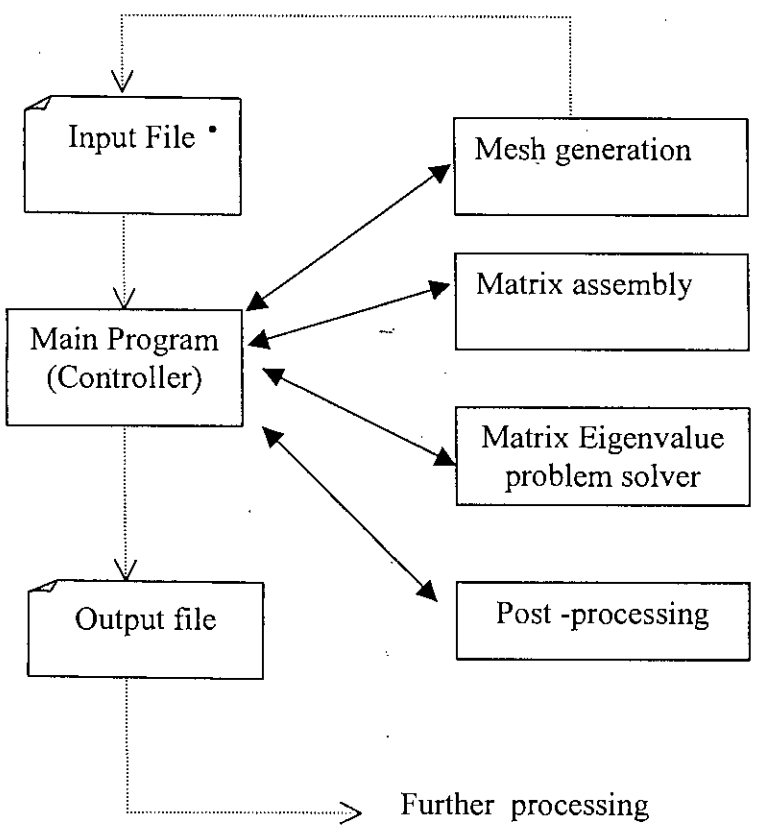

Fig. 5.1 Basic structure of the FEM program.

The program is formed of five parts: main program or controller, pre-processing part, matrix assembly part, eigenvalue solver part and post-processing part, as shown in Fig.5.1.

The main program or controller basically defines the options for running the program. These are of three kinds: input options, as for example whether to take input data from a pre-prepared file or from the pre-processor or mesh generator; solution options, in the matrix eigenvalue solver and loop parameters for repeated solution in the case where a dispersion curve is required; and output options, as for example the number of modes for which the field distribution is required as output for further processing.

The pre-processing part consists basically of a mesh generator and a module that establishes the boundary conditions. Mesh generation can be performed in different ways. Here in our program mesh generation is a simple, problem-dependent program which produces a topologically regular mesh of triangular elements The pre-processing part can also be run as an independent program to generate a file (to be used subsequently as an input file) containing the mesh definition with nodal description, permittivity profile and boundary conditions.

The matrix assembly part is the central part of the program. Its purpose is to construct the global matrices as the assembly of contributions for each element in the mesh. With the enforcement of boundary conditions, the global size of the assembled matrix is greatly reduced. The matrix eigenvalue solver is an implementation of the subspace iteration algorithm for complex, non-Hermitian matrices. It returns a number of selected eigenvalues and eigenvectors. The post-processing part calculates the propagation constants of the waveguide modes and, using the solution of the matrix solver and the boundary conditions, finds the corresponding field distribution. This part of the program also generates output files for further graphic processing of the solution, using standard packages. The field solutions from the output file are to be used with perturbation equations to find the loss when lossy waveguides are analyzed. This system has been tested using PCs with Pentium processor for a number of dielectric waveguides. The results will be shown for different lossless and lossy waveguides with step index profile.

5.2 NUMERICAL EXAMPLES

In order to check the accuracy of the FEM approach of this work, first consider a lossless rib waveguide having step index profile. By the symmetry of the system, half of the waveguide cross section can be divided into elements. For the structure shown in Fig. 5.2, we assume that λ_0=1.15 μm, $W = 3\,\mu m$, $t + h = 1.0\,\mu m$, $n_f = 3.44$, $n_s = 3.40$, and $n_c = 1.0$ and calculate the effective refractive index, $n_{eff} = \frac{\beta}{k_0}$, for the E_{11}^x and the E_{11}^y modes of the rib waveguide taking about 660 elements. The calculated values are

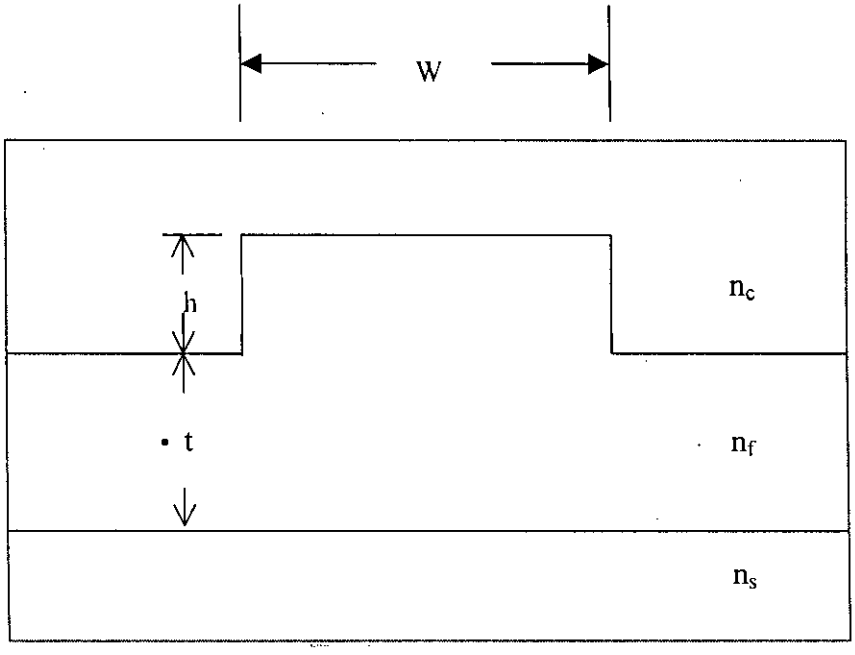

Fig. 5.2: Cross section of an optical rib waveguide.

shown in Table 5.1. Our result agree well with the results of the scalar finite element method (SFEM) and the scalar finite difference method (SFDM). Figs. 5.3, 5.4, 5.5, and 5.6 show plots of E_{11}^x, E_{21}^x, H_{11}^x, and H_{21}^x modes of the rib waveguide. Boundary conditions are properly applied to realize the modes. However, with the approach described here, the fundamental modes are efficiently calculated. As expected, the fields of fundamental modes are concentrated at the core region. In the calculation, we used symmetry of the structure and half of the cross section is divided into elements. This

reduced the size of the global matrices and required less memory space. Fig. 5.7 shows the refractive index versus h of the same rib waveguide. From this figure we can see that our result agree well with the results of SFEM and SFDM. The boundary conditions on the symmetry plane required for different mode calculations are given in Table 5.2.

TABLE 5.1: Effective refractive index of the E_{11}^{x} and E_{11}^{y} modes of a rib waveguides.

t (μm)	E_{11}^{x}			E_{11}^{y}		
	This work	SFDM	SFEM	This work	SFDM	SFEM
0.0	3.41106	3.41188	3.41204	3.41163	3.41051	3.41028
0.1	3.41225	3.41200	3.41214	3.41074	3.41060	3.41037
0.2	3.41253	3.41217	3.41229	3.41082	3.41073	3.41051
0.3	3.41263	3.41240	3.41249	3.41104	3.41092	3.41070
0.4	3.41282	3.41271	3.41276	3.41137	3.41117	3.41097
0.5	3.41328	3.41310	3.41311	3.41169	3.41150	3.41132
0.6	3.41368	3.41358	3.41353	3.41187	3.41190	3.41174
0.7	3.41423	3.41415	3.41404	3.41248	3.41241	3.41227
0.8	3.41478	3.41484	3.41468	3.41306	3.41303	3.41293
0.9	3.41567	3.41568	3.41553	3.41394	3.42385	3.41383

TABLE 5.2: Boundary conditions on the plane of symmetry for modal calculations.

Mode	**Symmetry plane**
E_{11}^{x}	Electric wall
H_{11}^{x}	Magnetic wall
E_{21}^{x}	Magnetic wall
H_{21}^{y}	Electric wall

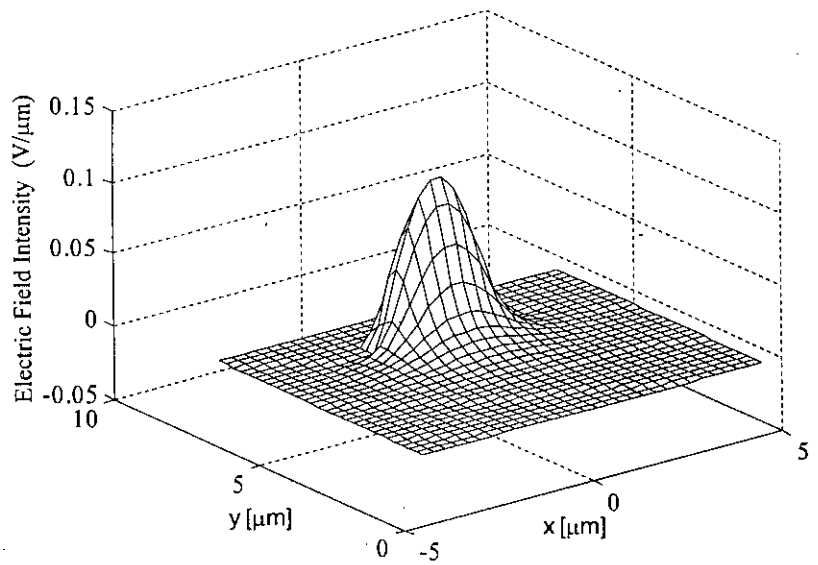

(a)

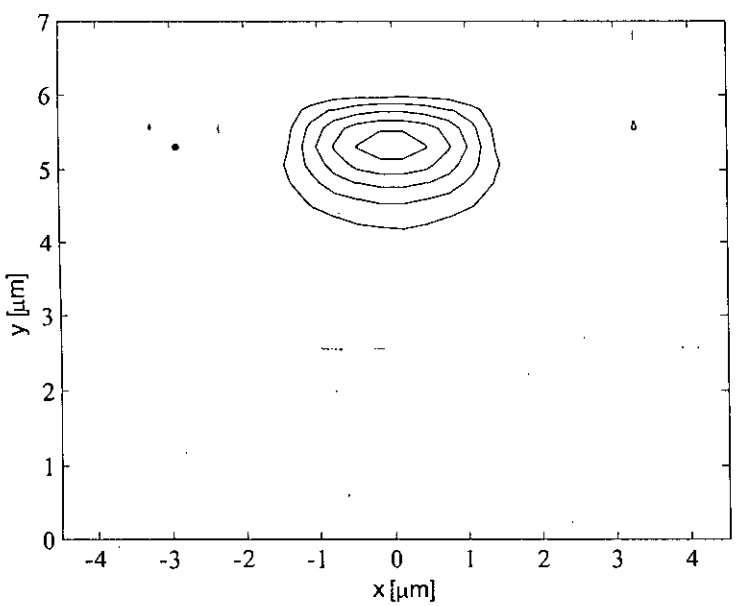

(b)

Fig. 5.3: E_{11}^{x} mode of the rib waveguide. (a) Surface plot. (b) Contour plot.

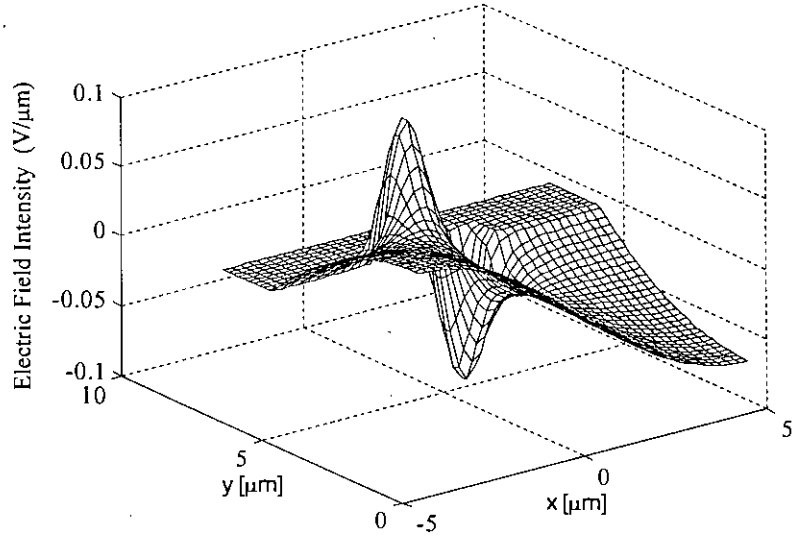

(a)

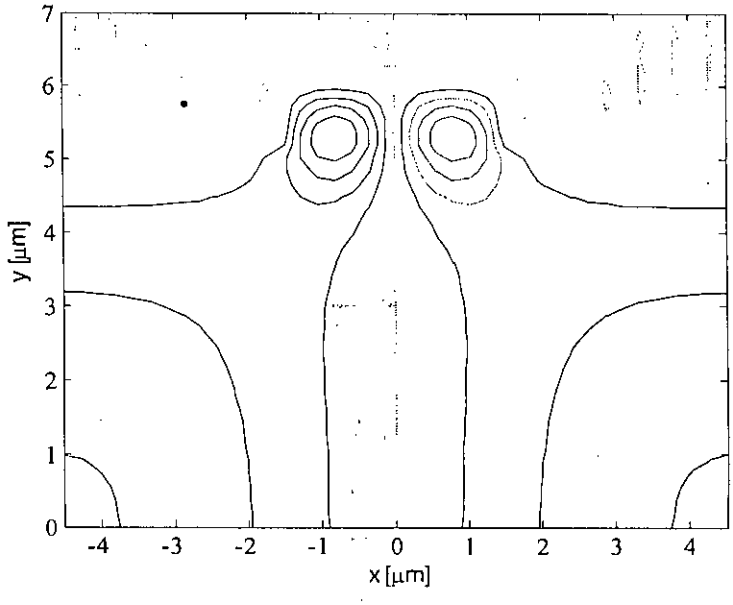

(b)

Fig. 5.4: E_{21}^{x} mode of the rib waveguide. (a) Surface plot. (b) Contour plot.

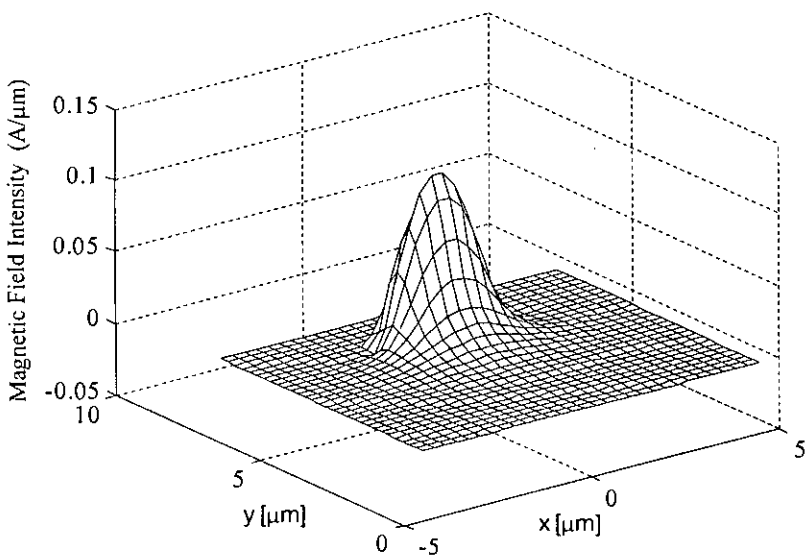

(a)

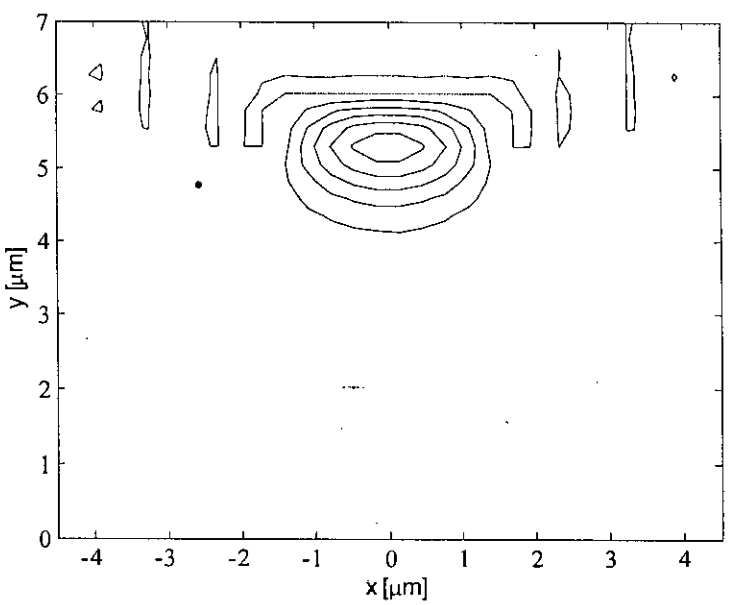

(b)

Fig. 5.5: H_{11}^{x} mode of the rib waveguide. (a) Surface plot. (b) Contour plot.

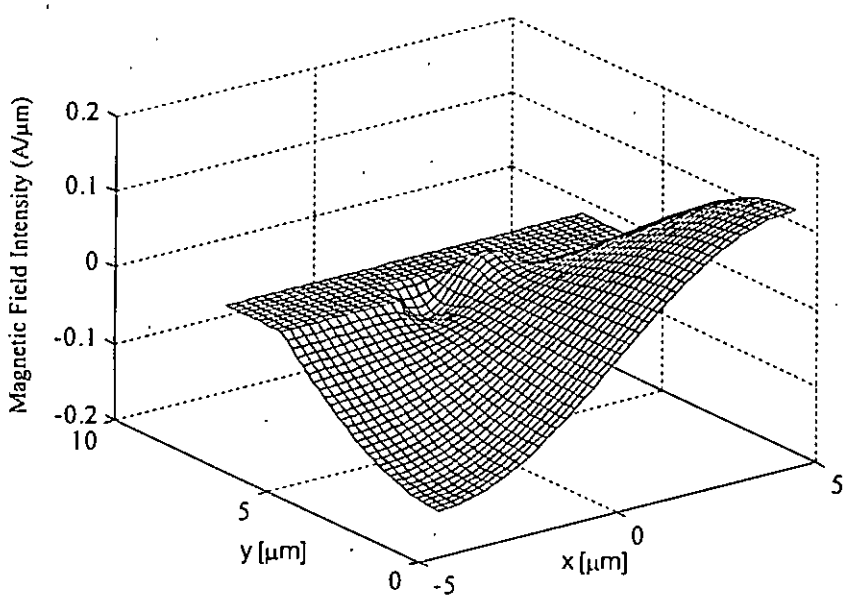

(a)

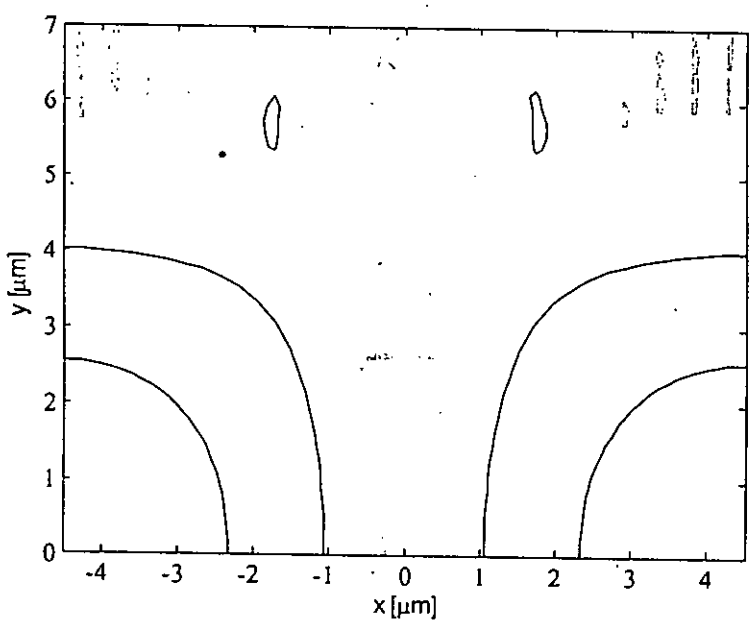

(b)

Fig. 5.6: H_{21}^{x} mode of the rib waveguide. (a) Surface plot. (b) Contour plot.

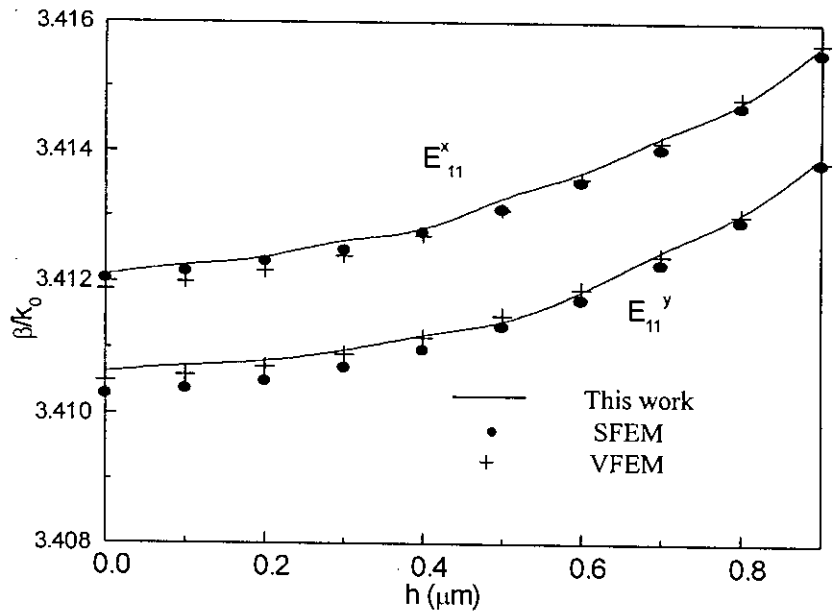

Fig. 5.7: The effective refractive index versus h of the rib waveguide.

Now let us consider a lossy optical rib waveguide. Fig. 5.8 shows an integrated laser rib waveguide with the active layer thickness, T=0.15 μm, n_0=1.0, n_1=3.38+j0.001 and n_2=3.17. Here the operating wavelength, λ = 1.5 μm. In the discretization process we take the half of the cross section using the symmetry plane of the structure along the y-axis as shown in Fig. 5.8. For this structure, we first consider that the refractive index n_1 is real, i.e., the structure is lossless. Using appropriate boundary condition on plane of symmetry, we first calculate the E_{11}^x (i.e., H_{11}^y) mode. Fig. 5.9 shows the contour plot of E_{11}^x mode for a height H of 0.6 μm. The contour plot shows similar to that of Fernandez and Lu [38]-[39]. Fig. 5.10 shows the variation of the normalized attenuation constant (α/k_0) and normalized phase constant (β/k_0) for the H_{11}^y mode with the thickness of the top confinement layer, H. The rib height is assumed to be very large. In this case we took the value 2.5 μm. The solid and dashed lines show the results of Lu and Fernandez [39], and our calculated values are shown by circles and dark circles. Good agreement can be observed between the results for the phase constant, while for the gain coefficient, although the trend is similar, the discrepancy is greater. This discrepancy could be due to the insufficient number of elements in the analysis.

•

We consider another example of Themistos *et. al.* [41]-[42]. In Fig. 5.11, we show the results. The solid line shows the result of our calculation. The dashed line and the dark circles show the results of a scalar FEM [41] and vector FEM [42], respectively. We can see that our result agree well with those of vector FEM [42]. Now we increase the active layer thickness, T, to 0.2 μm and re-examine the rib waveguide of the previous example. Fig. 5.12 shows the normalized attenuation constant for the dominant TE_{11} (E_{11}^x) mode with the thickness of the top confinement layer, H. The solid line shows our result and the dark circles show the results of Themistos *et. al.* [42]. We can see that our result agree well with the results of Themistos *et. al.* [42] in this case also. So, all these verify that our approach is giving satisfactory results for the loss constant. As a matter of fact, if the imaginary part of the refractive index is positive, the material is said to have gain and then α is called the gain coefficient.

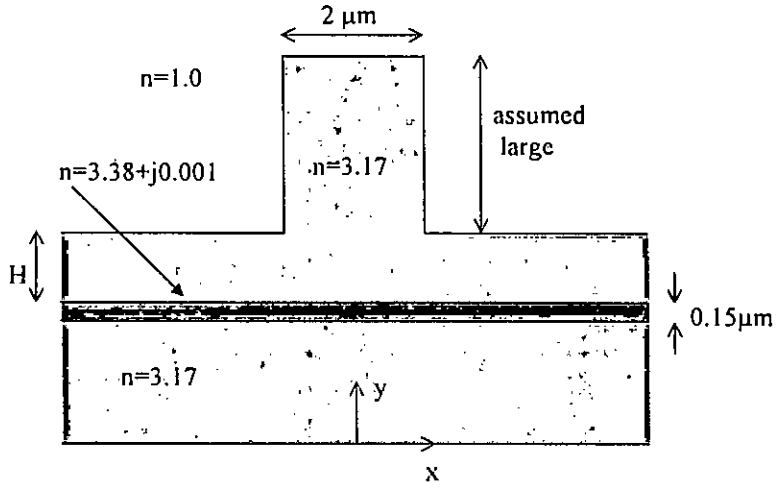

Fig. 5.8: Cross section of integrated laser rib waveguide.

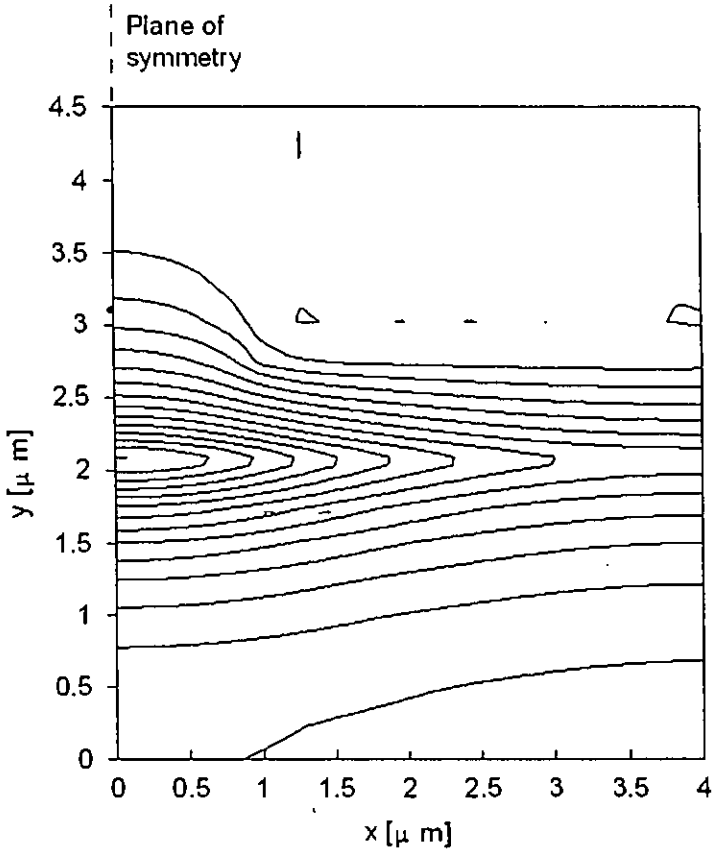

Fig. 5.9: Contour plot of the E_{11}^{x} (i.e., H_{11}^{y}) mode.

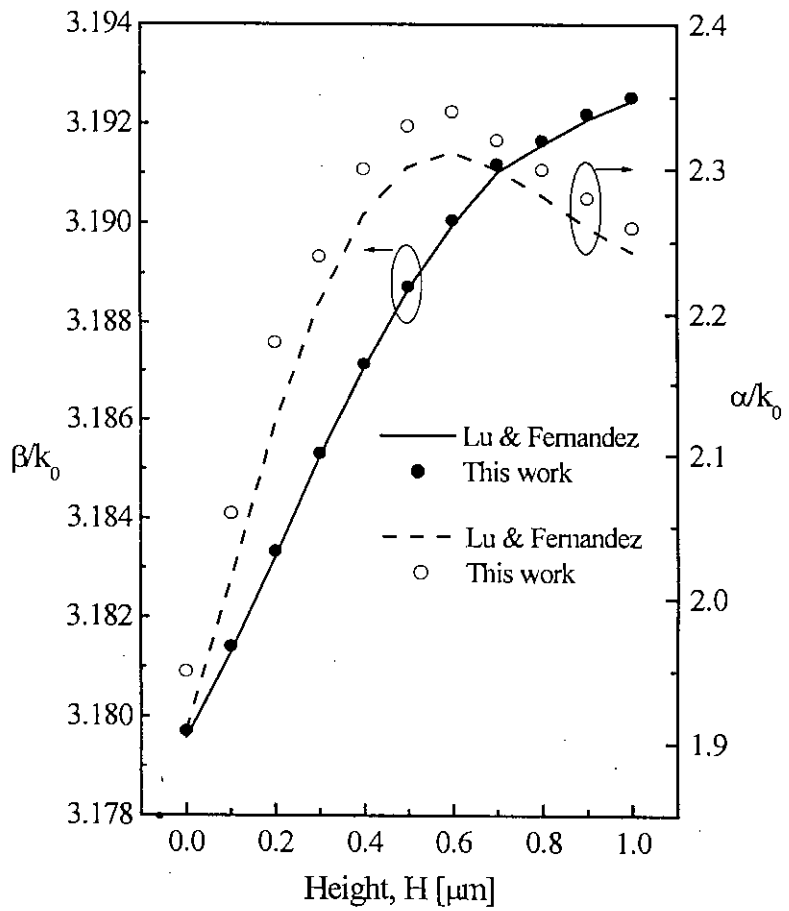

Fig. 5.10: Normalized propagation constant (attenuation and phase constants) for the dominant H_{11}^{y} mode versus the height H.

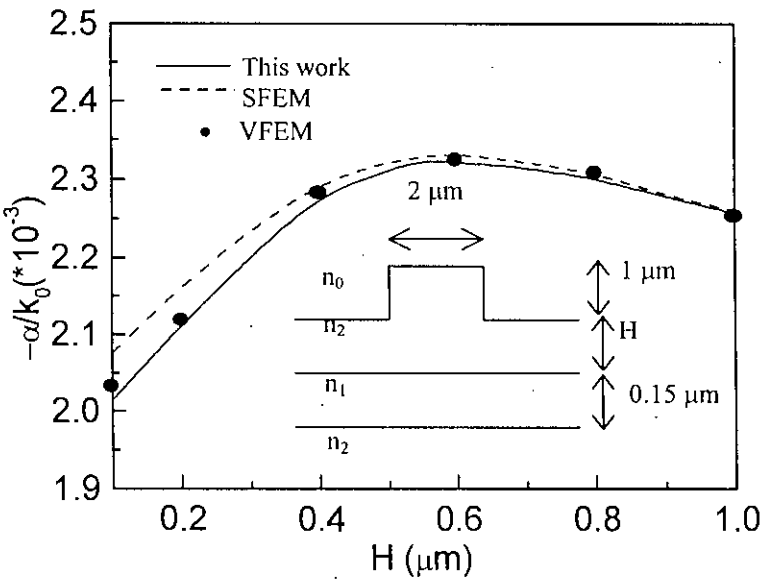

Fig. 5.11: Variation of the gain constant versus top confinement layer thickness of a semicinductor laser rib waveguide.

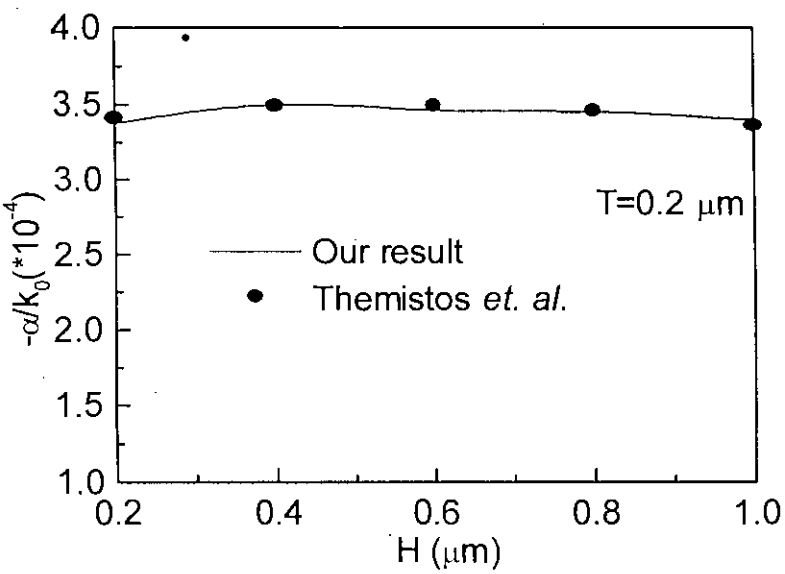

Fig. 5.12: Variation of normalized gain with the top confinement layer *H*.

Next, we consider a lossy dielectric waveguide (an embedded channel waveguide) as shown in Fig. 5.13. In this work, the width of the active region, W, is five times greater than the height of the active layer, d. Here, in this example, the imaginary part of the core refractive index is positive, *i.e.*, n_1=3.5+j10^{-3}, indicating a gain medium and that of the substrate region is negative, *i.e.*, n_2=3.2-jn_2'', indicating a loss in that region. Variations of the normalized modal gain g/k_0 (*i.e.*, $-\alpha / k_0$) with the normalized waveguide dimension ($k_0 d$) for different negative imaginary values (with loss) of the cladding refractive index are shown in Fig. 5.14 for the fundamental H_{11}^{y} (*i.e.*, TE_{11}) mode. Results obtained using our approach agree well with the results of Themistos *et. al* [42]. The solid lines in the figure indicate our result and the dark circles show the results of Themistos *et. al.* [42]. Even though, we can observe a difference between our result and those of Themistos *et. al.* for n_2''=10^{-2} in the figure, we believe that this could be due to insufficient number of elements in the calculation.

Finally, we consider another example of a dielectric block loaded rectangular waveguide as shown in Fig. 5.15. The refractive index of the dielectric block is given by $\varepsilon_r = \varepsilon_{rr} - j1.5$. For this case, the whole cross section is used in the analysis. As usual, the boundary is a perfect electrical wall. Fig. 5.16 and Fig. 5.17 show the normalized phase constant and the normalized attenuation constant, respectively. For phase constant our results agree well with those of Sheng and Xu [44]. Also, it can be observed that loss is greater for smaller values of the real part of the complex refractive index.

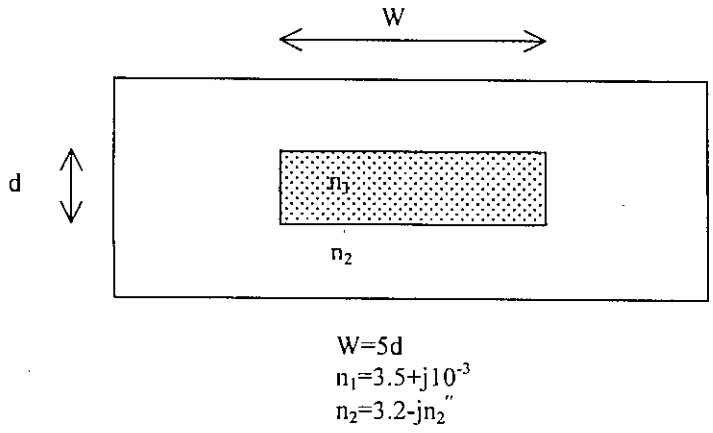

Fig. 5.13: Cross section of an embedded channel waveguide.

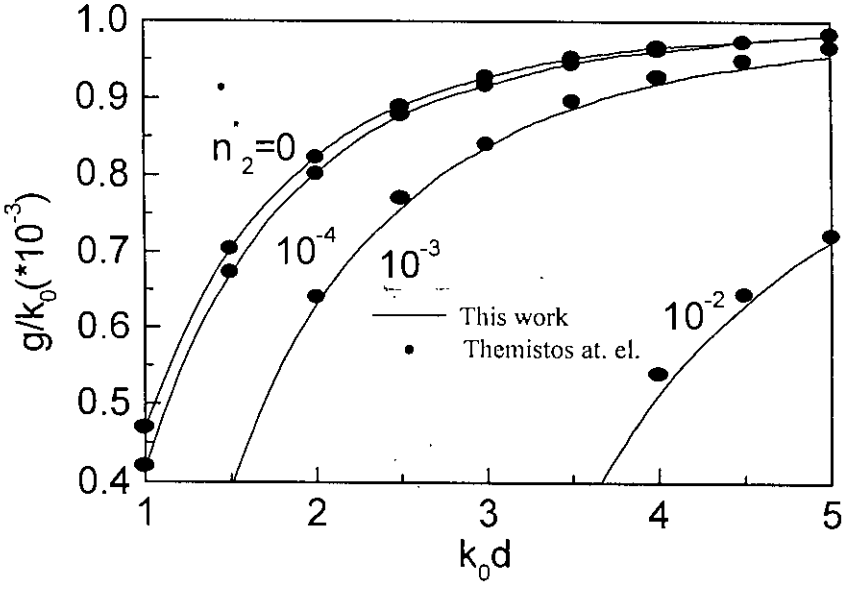

Fig. 5.14: Variation of modal gain versus normalized dimension for the TE_{11} mode of an embedded channel waveguide.

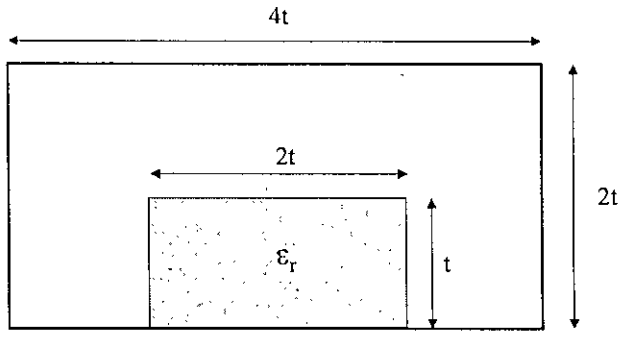

Fig. 5.15: Cross section of a dielectric block loaded rectangular waveguide.

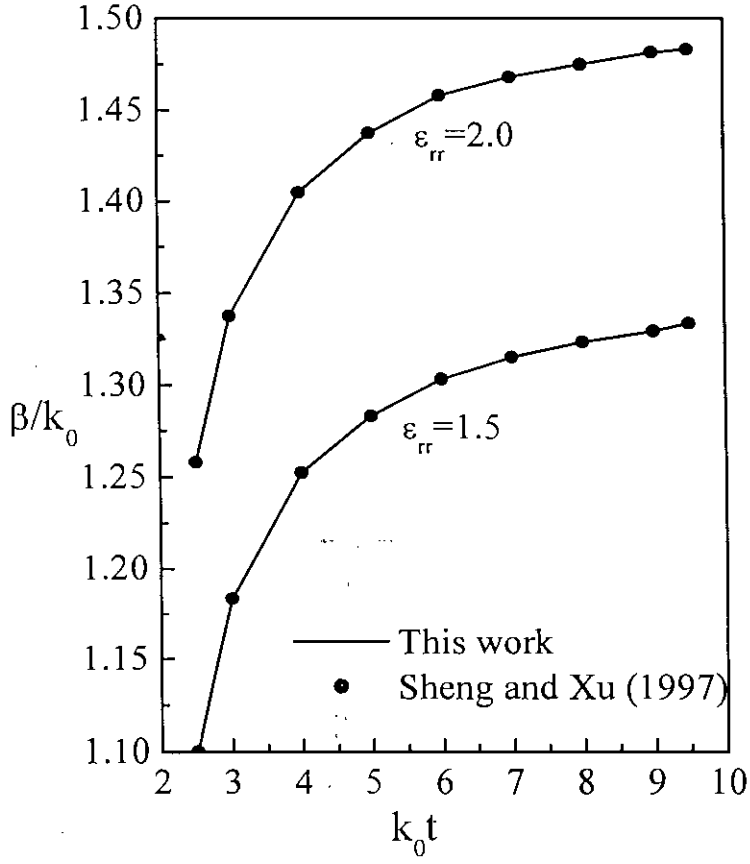

Fig. 5.16: Normalized phase constant of E_{11}^y mode of the dielectric block loaded rectangular waveguide.

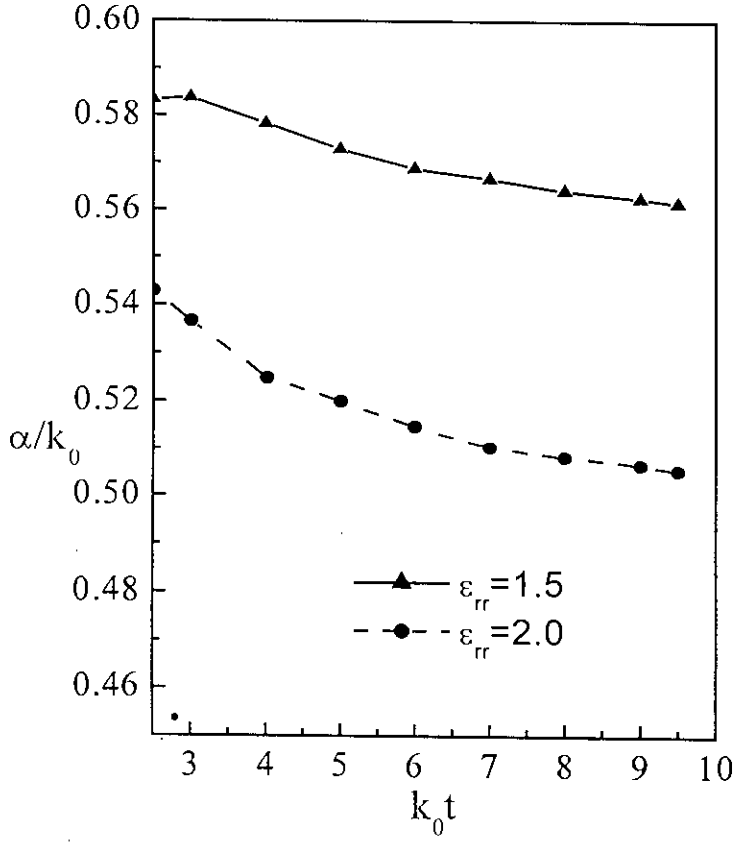

Fig. 5.17: Normalized attenuation constant of E_{11}^{y} mode of the dielectric block loaded rectangular waveguide.

Chapter 6

CONCLUSION

6.1 SUMMARY

The finite element method has become a powerful tool for the analysis of electromagnetic waveguide problems. Different vector and scalar wave formulations are there in the literature for the analysis of electromagnetic dielectric waveguide and some of them are reviewed in the introduction of this thesis. Here in this work, a very efficient vector wave based finite element technique is formulated for the analysis of lossless and lossy dielectric waveguides.

•

Hybrid edge/nodal type triangular elements are employed here with the finite element approach in this work. The formulation is modified to give an eigenvalue equation, where sparsity of final matrices can be exploited and high-speed computation is possible. An indirect approach based on perturbation technique is presented here for the calculation of loss of optical waveguides. The methods are implemented on Pentium-II and Pentium-III computers and useful numerical results are calculated for slab loaded dielectric waveguides, rectangular waveguides and optical rib waveguides. The results agreed well with the previously published results.

Since the approach here is developed to give solutions of propagation constants directly as eigenvalue and fields as eigenvector for a given frequency, the method can be employed to many complex structures for modal analysis. The analysis also ensures true hybrid mode propagation through the use of hybrid edge/nodal elements. Thus, the analysis here reveals that the approach is very simple and efficient for the solution of

lossless and lossy optical waveguides. Also, the system developed eliminates the need to solve complex eigenvalue problem when complex eigenvalue solver is unavailable. Numerical methods are usually evaluated in terms of their generality, accuracy, efficiency, and complexity. But most of the numerical techniques represent some sort of compromise between these aspects. No method is superior to the other in all aspects. However, our present approach is rather efficient and provide very good accuracy. Accurate computer analysis of waveguide devices are always needed today with the growing intricacy in integrated circuits. So, the systems developed in this work may be incorporated to produce an efficient CAD system.

6.2 SUGGESTIONS FOR FUTURE WORK

Since the system developed in this work is found to be very efficient, the system can be generalized for general anisotropic waveguides with full permittivity and permeability tensors.

As for the elements the interpolating functions may be modified to build hybrid edge/nodal curvilinear elements so that they can be used to accommodate them in the curved boundaries of arbitrary cross sectional structures.

Furthermore, all these systems may be incorporated to produce an efficient CAD system for optical integrated circuits.

References

[1] K. Okamoto, *Fundamentals of Optical Waveguides*, Academic Press, 2000.

[2] R.E. Collin, *Field Theory of Guided Waves*, New York: IEEE Press, 1991.

[3] P. P. Silvester and R. L. Ferrari, *Finite Elements for Electrical Engineers*, Cambridge University Press, Second ed., 1990.

[4] J. Jin, *The Finite Element Method in Electromagnetics*, John Wiley & Sons, Inc., 1993.

[5] S. Ramo, J. R. Whinnery, and T. V. Duzer, *Fields and waves in communication Electronics*, John wiley & Sons, Inc., 1990.

[6] D. Marcuse, *Theory of Dielectric Optical Waveguides*, Academic Press, Inc., Second ed., 1991.

[7] M. Koshiba, *Optical Waveguide Analysis*, McGraw-Hill, Inc., 1992.

[8] M. Koshiba, *Optical Waveguide Theory by the Finite Element Method*, Kluwer Academic Publisher, 1992.

[9] A. Konard, "High-order triangular finite elements for electromagnetic waves in anisotropic media," *IEEE Trans. Microwave Theory Tech.*, vol. **MTT-25**, pp. 353-360, May 1977.

[10] M. Koshiba, K. Hayata, and M. Suzuki, "Approximate scalar finite element analysis of anisotropic optical waveguides with off-diagonal elements in a permittivity tensor," *IEEE Trans. Microwave Theory Tech.*, vol. **MTT-32**, pp. 587-593, June 1984.

[11] B. M. A. Rahman and J. B. Davies, "Finite element analysis of optical and microwave waveguide problem," *IEEE Trans. Microwave Theory Tech.*, vol. **MTT-32**, pp. 20-28, Jan. 1984.

[12] B. M. A. Rahman and J. B. Davies, "Penalty function improvement of waveguide solution by finite elements," *IEEE Trans. Microwave Theory Tech.,* vol. **MTT-32**, no. 8, pp. 922-928, Aug. 1984.

[13] M. Hano, "Finite-element analysis of dielectric-loaded waveguides," *IEEE Trans. Microwave Theory Tech.,* vol. **MTT-32**, no. 10, pp. 1275-1279, Oct.1984.

[14] M. Koshiba, K. Hayata, and M. Suzuki, "Finite element-formulation in terms of the electric field vector for electromagnetic waveguide problem," *IEEE Trans. Microwave Theory Tech.*, vol. **MTT-33**, no. 10, pp. 900-905, Oct. 1985.

[15] M. Koshiba, K. Hayata and M. Suzuki, "Improved finite-element formulation in terms of the magnetic field vector for dielectric waveguides," *IEEE Trans. Microwave Theory Tech.,* vol. **MTT-33**, no. 3, pp. 227-233, Mar. 1985.

[16] J. A. M. Svedin, "A numerically efficient finite-element formulation for the general waveguide problem without spurious modes," *IEEE Trans. Microwave Theory Tech.,* vol. 37, pp. 1708-1715, Nov. 1989.

[17] K. Hayata, M. Koshiba, M. Eguchi, and M. Suzuki, "Vectorial finite-element method without any spurious solution for dielectric waveguiding problems using transverse magnetic-field component," *IEEE Trans. Microwave Theory Tech.*, vol. **MTT-34**, no. 11, pp. 1120-1124, Nov. 1986.

[18] T. Angkaew, M. Matsuhara, and N. Kumagai, "Finite-element analysis of waveguide modes: A novel approach that eliminates spurious modes," *IEEE Trans. Microwave Theory Tech.*, vol. **MTT-35**, no. 2, pp. 117-123, Feb. 1987.

[19] F. A. Fernandez and Y. Lu, "Variational finite-element analysis of dielectric waveguides with no spurious solutions," *Electron. Lett.,* vol. 26, no. 25, pp. 2125-2126, 1990.

[20] F. A. Fernandez and Y. Lu, "A variational finite-element formulation for dielectric waveguides in terms of transverse magnetic fields," *IEEE Trans on Magnetics,* vol. **MAG- 27**, no. 5, pp. 3864-3867, Sept. 1991.

[21] B. M. A. Rahman, F. A. Fernandez, and J. B. Davies, "Review of finite element methods for microwave and optical waveguides," *Proc. IEEE,* vol.79, pp. 1442-1448, Oct. 1991.

[22] J. B. Davies, " Finite Element Analysis of waveguides Cavaties – a Review," *IEEE Trans. on Magnetics,* vol. 29, no. 2, Mar. 1993.

[23] K. S. Chiang, "Review of numerical and approximate methods for the modal analysis of general optical dielectric waveguides," *Optical and Quantum Electronics*, 26, pp. 113-134, 1994.

[24] J. -F Lee, D. K. Sun, and Z. J. Cendes, "Full-wave analysis of dielectric waveguides using tangential vector finite elements," *IEEE Trans. Microwave Theory Tech.,* vol. **MTT-39**, no. 8, pp. 1262-1271, Aug. 1991.

[25] J. -F Lee, D. K. Sun, and Z. J. Cendes, "Tangential vector finite-elements for electromagnetic field computation," *IEEE Trans. Magnetics,* vol. **MAG-27**, pp. 4032-4035, Sept. 1991.

[26] M. Koshiba and K. Inoue, "Simple and efficient finite-element analysis of microwave and optical waveguides," *IEEE Trans. Microwave Theory Tech.,* vol. 40, no. 2, pp. 371-377, Feb. 1992.

[27] M. Koshiba, S. Maruyama, and K. Hirayama, "A vector finite element method with the high-order mixed-interpolation-type triangular elements for optical waveguiding problems," *J. Lightwave Technol.*, vol.12, no.3, pp. 495-502, Mar. 1994.

[28] M. Koshiba, "Finite element method for modeling lossy planar transmission lines with arbitrary cross section," *Asia Pacific Microwave Conference Proceedings,* vol. III, no. 32-1, pp. 909-912, 1994.

[29] J. P. Webb, " Edge elements and what they can do for you," *IEEE Trans. Magnet.,* vol. 29, pp. 1460-1465, Mar. 1993.

[30] B. M. Dillon and J. P. Webb, "A comparison of formulations for the vector finite element analysis of waveguides," *IEEE Trans. Microwave Theory Tech.*, vol. 42, pp. 308-316, Feb. 1994.

[31] M. S. Alam, K. Hirayama, Y. Hayashi, and M. Koshiba, " Finite element analysis of propagating, evanescent, and complex modes in finlines," *IEE Proceedings on Microwaves, Antennas and propagation, Part H,* vol. 141, no.2, pp. 65-69, Apr. 1994.

[32] M. S. Alam, M. Koshiba, K. Hirayama, and Y. Hayashi, "Analysis of lossy planar transmission lines by using a vector finite element method," *IEEE Trans. on Microwave Theory Tech.*, vol. 43, no. 10, pp. 2466-2471, Oct. 1995.

[33] A. C. Polycarpou, M. R. Lyons, and C. A. Balanis, "Finite Element Analysis of MMIC Waveguide structures with Anisotropic substrates," *IEEE Trans. on Microwave Theory Tech.*, vol. 44, no. 10, pp. 1650-1663, Oct. 1996.

[34] M. Matsuhara, H. Yunoki, and A. Murata, " Analysis of open type waveguides by the vector finite-element method," *IEEE Microwave Guided Wave Lett.*, vol.1, pp.376-378, Dec. 1991.

[35] L. Valor and J. Zapata, " Efficient Finite Element Analysis of waveguides with lossy inhomogeneous anisotropic materials characterized by arbitrary permittivity and permeability tensors," *IEEE Trans. on Microwave Theory and Tech.*, vol. 43, no. 10, Oct. 1995.

[36] P. K. Mishra and A. Sharma, " Analysis of single mode inhomogeneous planar waveguides," *J. Lightwave Technol.*, vol. LT-4. pp. 204-212, Feb. 1986.

[37] E. M. Conwell, " Modes in optical waveguides formed by diffusion," *Appl. Phys. Lett.*, vol. 23, no. 6, pp. 328-329, 1973.

[38] F. A. Fernandez and Y. Lu, Microwave and Optical Waveguide Analysis by the Finite Element Method, Research Studies Press Ltd., 1996.

[39] Y. Lu, and F. A. Fernandez, "Vector finite element analysis of integrated optical waveguides," *IEEE Trans. Magn.*, vol. 30, pp. 3116-3119, Sept. 1998.

[40] K. Hayata, M. Koshiba, and M. Suzuki, "Lateral mode analysis of buried heterostructure diode lasers by the finite element method," *IEEE J. Quantum Electron.*, vol. QE-22, no. 6, pp. 781-788, June 1986.

[41] C. Themistos, B.M.A. Rahman, and K.T.V. Grattan, "Finite Element Analysis for Lossy Optical Waveguides by Using Perturbation Techniques," *IEEE Photonics Technol. Lett.*, vol. 6, no. 4, pp. 537-539, Apr. 1998.

[42] C. Themistos, B.M.A. Rahman, A. Hadjicharalambous, and K.T.V. Grattan, "Loss/Gain Characterization of Optical Waveguides," *J. Lightwave Technol.*, vol. 13, no. 8, pp. 1760-1765, Aug. 1998.

[43] M. S. Alam, K. Hirayama, Y. Hayashi, and M. Koshiba, "Analysis of shielded microstrip lines with arbitrary metallization cross section using a vector finite element method," *IEEE Trans. Microwave Theory Tech.*, vol. 42, no. 11, pp. 2112-2117, Nov. 1994.

[44] X. –Q. Sheng and S. Xu, "An Efficient High-Order Mixed-Edge Rectangular Element Method for Lossy Anisotropic Dielectric Waveguides," *IEEE Trans. Microwave Theory Tech.*, vol. 45, no. 7, pp. 1009-1013, July 1997.

[45] P. Savi, I.-L. Gheorma, and R. D. Graglia, "Full-Wave High-Order FEM Model for Lossy Anisotropic Waveguides," *IEEE Trans. Microwave Theory Tech.*, vol. 50, no. 2, pp. 495-500, Feb. 2002.

[46] Z. Pantic, and R. Mittra, "Quasi-TEM analysis of microwave transmission lines by the finite element method," *IEEE Trans. Microwave Theory Tech.*, vol. MTT-34, pp. 1096-1103, Nov. 1996.

[47] M. R. Islam and M. S. Alam, "Calculation of Loss in Optical Waveguides Using Finite Element Method and Perturbation Technique," pp. 360-363, *Proceedings of Second International Conference on Electrical and Computer Engineering ICECE 2002,* Dhaka, Bangladesh, Dec. 2002.

Appendix

A. Lowest order element

$$\left[\iint_e \{U\}\{U\}^T dxdy\right]_{ij}$$
$$= \frac{1}{4A_e} l_i l_j \left[y_{i+2} y_{j+2} - y_c \left(y_{i+2} + y_{j+2}\right) + \frac{1}{12}\left(y_1^2 + y_2^2 + y_3^2 + 9y_c^2\right)\right]$$

$$\left[\iint_e \{V\}\{V\}^T dxdy\right]_{ij}$$
$$= \frac{1}{4A_e} l_i l_j \left[x_{i+2} x_{j+2} - x_c' \left(x_{i+2} + x_{j+2}\right) + \frac{1}{12}\left(x_1^2 + x_2^2 + x_3^2 + 9x_c^2\right)\right]$$

$$\left[\iint_e \{U_y\}\{U_y\}^T dxdy\right]_{ij}$$
$$= \left[\iint_e \{V_x\}\{V_x\}^T dxdy\right]_{ij}$$
$$= -\left[\iint_e \{U_y\}\{V_x\}^T dxdy\right]_{ij}$$
$$= -\left[\iint_e \{V_x\}\{U_y\}^T dxdy\right]_{ij}$$
$$= \frac{1}{4A_e} l_i l_j$$

$$\left[\iint_e \{U\}\{N_x\}^T dxdy\right]_{ij} = \frac{1}{4A_e} l_i b_j (y_{i+2} - y_c)$$

$$\left[\iint_e \{V\}\{N_y\}^T dxdy\right]_{ij} = \frac{1}{4A_e} l_i c_j (x_c - x_{i+2})$$

$$\left[\iint_e \{N\}\{N\}^T dxdy\right]_{ij} = \begin{cases} A_e/6 & for\ i = j \\ A_e/12 & for\ i \neq j \end{cases}$$

$$\left[\iint_e \{N_x\}\{N_x\}^T dxdy\right]_{ij} = \frac{1}{4A_e} b_i b_j$$

$$\left[\iint_e \{N_y\}\{N_y\}^T dxdy\right]_{ij} = \frac{1}{4A_e} c_i c_j$$

with

$$x_c = (x_1 + x_2 + x_3)/3$$
$$y_c = (y_1 + y_2 + y_3)/3$$

where $[\ .\ ]_{ij}\,(ij = 11,12,.....,33)$ indicates the (i, j) components of the matrix [.], and the subscripts i, j always progress modulo 3.

B. Higher order element

$$\left[\iint_e \{U\}\{U\}^T dxdy\right]_{ij}$$

$$= \begin{cases} \frac{A_e}{6} u_i u_j \ \ for \ \ ij = 11, 22, 33, 44, 55, 66, 16, 61, 24, 42, 35, 53 \\ \frac{A_e}{12} u_i u_j \ \ for \ \ others \end{cases}$$

$$\left[\iint_e \{V\}\{V\}^T dxdy\right]_{ij}$$

$$= \begin{cases} \frac{A_e}{6} v_i v_j \ \ for \ \ ij = 11, 22, 33, 44, 55, 66, 16, 61, 24, 42, 35, 53 \\ \frac{A_e}{12} v_i v_j \ \ for \ \ others \end{cases}$$

$$\left[\iint_e \{U_y\}\{U_y\}^T dxdy\right]_{ij} = A_e u_{yi} u_{yj}$$

$$\left[\iint_e \{V_x\}\{V_x\}^T dxdy\right]_{ij} = A_e v_{xi} v_{xj}$$

$$\left[\iint_e \{U_y\}\{V_x\}^T dxdy\right]_{ij} = A_e u_{yi} v_{xi}$$

$$\left[\iint_e \{V_x\}\{U_y\}^T dxdy\right]_{ij} = A_e v_{xi} u_{yi}$$

$$\left[\iint_e \{V\}\{N_y\}^T dxdy\right]_{4j} = \frac{A_e}{12} v_4 \left(C_{yj}^{(1)} + 2C_{yj}^{(2)} + C_{yj}^{(3)} + 4C_{yj}^{(4)}\right)$$

$$\left[\iint_e \{V\}\{N_y\}^T dxdy\right]_{5j} = \frac{A_e}{12} v_5 \left(C_{yj}^{(1)} + C_{yj}^{(2)} + 2C_{yj}^{(3)} + 4C_{yj}^{(4)}\right)$$

$$\left[\iint_e \{V\}\{N_y\}^T dxdy\right]_{6j} = \frac{A_e}{12} v_6 \left(2C_{yj}^{(1)} + C_{yj}^{(2)} + C_{yj}^{(3)} + 4C_{yj}^{(4)}\right)$$

$$\left[\iint_e \{U\}\{N_x\}^T dxdy\right]_{1j} = \frac{A_e}{12} u_1 \left(2C_{xj}^{(1)} + C_{xj}^{(2)} + C_{xj}^{(3)} + 4C_{xj}^{(4)}\right)$$

$$\left[\iint_e \{U\}\{N_x\}^T dxdy\right]_{2j} = \frac{A_e}{12} u_2 \left(C_{xj}^{(1)} + 2C_{xj}^{(2)} + C_{xj}^{(3)} + 4C_{xj}^{(4)}\right)$$

$$\left[\iint_e \{U\}\{N_x\}^T dxdy\right]_{3j} = \frac{A_e}{12} u_3 \left(C_{xj}^{(1)} + C_{xj}^{(2)} + 2C_{xj}^{(3)} + 4C_{xj}^{(4)}\right)$$

$$\left[\iint_e \{U\}\{N_x\}^T dxdy\right]_{4j} = \frac{A_e}{12} u_4 \left(C_{xj}^{(1)} + 2C_{xj}^{(2)} + C_{xj}^{(3)} + 4C_{xj}^{(4)}\right)$$

$$\left[\iint_e \{U\}\{N_x\}^T dxdy\right]_{5j} = \frac{A_e}{12} u_5 \left(C_{xj}^{(1)} + C_{xj}^{(2)} + 2C_{xj}^{(3)} + 4C_{xj}^{(4)}\right)$$

$$\left[\iint_e \{U\}\{N_x\}^T dxdy\right]_{6j} = \frac{A_e}{12} u_6 \left(2C_{xj}^{(1)} + C_{xj}^{(2)} + C_{xj}^{(3)} + 4C_{xj}^{(4)}\right)$$

$$\left[\iint_e \{V\}\{N_y\}^T dxdy\right]_{1j} = \frac{A_e}{12} v_1 \left(2C_{yj}^{(1)} + C_{yj}^{(2)} + C_{yj}^{(3)} + 4C_{yj}^{(4)}\right)$$

$$\left[\iint_e \{V\}\{N_y\}^T dxdy\right]_{2j} = \frac{A_e}{12} v_2 \left(C_{yj}^{(1)} + 2C_{yj}^{(2)} + C_{yj}^{(3)} + 4C_{yj}^{(4)}\right)$$

$$\left[\iint_e \{V\}\{N_y\}^T dxdy\right]_{3j} = \frac{A_e}{12} v_3 \left(C_{yj}^{(1)} + C_{yj}^{(2)} + 2C_{yj}^{(3)} + 4C_{yj}^{(4)}\right)$$

$$\iint_e \{N\}\{N\}^T dxdy = \frac{A_e}{180} \begin{bmatrix} 6 & -1 & -1 & 0 & -4 & 0 \\ -1 & 6 & -1 & 0 & 0 & -4 \\ -1 & -1 & 6 & -4 & 0 & 0 \\ 0 & 0 & -4 & 32 & 16 & 16 \\ -4 & 0 & 0 & 16 & 32 & 16 \\ 0 & -4 & 0 & 16 & 16 & 32 \end{bmatrix}$$

$$\left[\iint_e \{N_x\}\{N_x\}^T dxdy\right]_{ij} = \frac{A_e}{6}\left(C_{xi}^{(1)}C_{xj}^{(1)} + C_{xi}^{(2)}C_{xj}^{(2)} + C_{xi}^{(3)}C_{xj}^{(3)}\right)$$

$$+\frac{A_e}{12}\left(C_{xi}^{(1)}C_{xj}^{(2)} + C_{xi}^{(1)}C_{xj}^{(3)} + C_{xi}^{(2)}C_{xj}^{(1)} + C_{xi}^{(2)}C_{xj}^{(3)} + C_{xi}^{(3)}C_{xi}^{(1)} + C_{xi}^{(3)}C_{xj}^{(2)}\right)$$

$$\frac{A_e}{3}\left(C_{xi}^{(1)}C_{xj}^{(4)} + C_{xi}^{(2)}C_{xj}^{(4)} + C_{xi}^{(3)}C_{xj}^{(4)} + C_{xi}^{(4)}C_{xj}^{(1)} + C_{xi}^{(4)}C_{xi}^{(2)} + C_{xi}^{(4)}C_{xj}^{(3)}\right) + A_e C_{xi}^{(4)}C_{xj}^{(4)}$$

$$\left[\iint_e \{N_y\}\{N_y\}^T dxdy\right]_{ij} = \frac{A_e}{6}\left(C_{yi}^{(1)}C_{yj}^{(1)} + C_{yi}^{(2)}C_{yj}^{(2)} + C_{yi}^{(3)}C_{yj}^{(3)}\right)$$

$$+\frac{A_e}{12}\left(C_{yi}^{(1)}C_{yj}^{(2)} + C_{yi}^{(1)}C_{yj}^{(3)} + C_{yi}^{(2)}C_{yj}^{(1)} + C_{yi}^{(2)}C_{yj}^{(3)} + C_{yi}^{(3)}C_{yi}^{(1)} + C_{yi}^{(3)}C_{yj}^{(2)}\right)$$

$$\frac{A_e}{3}\left(C_{yi}^{(1)}C_{yj}^{(4)} + C_{yi}^{(2)}C_{yj}^{(4)} + C_{yi}^{(3)}C_{yj}^{(4)} + C_{yi}^{(4)}C_{yj}^{(1)} + C_{yi}^{(4)}C_{yi}^{(2)} + C_{yi}^{(4)}C_{yj}^{(3)}\right) + A_e C_{yi}^{(4)}C_{yj}^{(4)}$$

where $[\,.\,]_{ij}$ (ij= 11,12,.....66) indicates the ($i.j$) components of the matrix [.], and the values of u_i, v_i, u_{yi}, v_{xi} and $C_{xi}^{(1)}$ to $C_{yi}^{(4)}$ are listed in Table A1.

Table A 1 : Values of u_i, v_i, u_{yi}, v_{xi} and $C_{xi}^{(1)}$ to $C_{yi}^{(4)}$

i	u_i	v_i	u_{yi}	v_{xi}	$C_{xi}^{(1)}$	$C_{xi}^{(2)}$	$C_{xi}^{(3)}$	$C_{xi}^{(4)}$	$C_{yi}^{(1)}$	$C_{yi}^{(2)}$	C_{yi}^{3}	$C_{yi}^{(4)}$
1	l_1b_2	l_1c_2	u_1c_1	v_1b_1	$4b_1$	0	0	$-b_1$	$4c_1$	0	0	$-c_1$
2	l_2b_3	l_2c_3	u_2c_2	v_2b_2	0	$4b_2$	0	$-b_2$	0	$4c_2$	0	$-c_2$
3	l_3b_1	l_3c_1	u_3c_3	v_3b_3	0	0	$4b_3$	$-b_3$	0	0	$4c_3$	$-c_3$
4	$-l_1b_1$	$-l_1c_1$	u_4c_2	v_4b_2	$4b_2$	$4b_1$	0	0	$4c_2$	$4c_1$	0	0
5	$-l_2b_2$	$-l_2c_2$	u_5c_3	v_5b_3	0	$4b_3$	$4b_2$	0	0	$4c_3$	$4c_2$	0
6	$-l_3b_3$	$-l_3c_3$	u_6c_1	v_6b_1	$4b_3$	0	$4b_1$	0	$4c_3$	0	$4c_1$	0

C. Numerical Integration

Finite element methods are always based on integral formulations. For some cases the integration's are possible and the algebraic expressions can be obtained easily. However, in some cases, e.g., graded-index profiles, it is impossible to integrate the expression in closed form. Then the use of numerical integration is a must. Also, elements with curved or distorted sides, it is always necessary to use numerical integration. The use of numerical integration avoids lengthy algebraic expressions and simplifies the programming of the element matrices.

For an integral over a triangular element, Hammer's formula follows

$$\iint_{\Delta} f(L_1, L_2, L_3)\, dx\, dy = \sum_{i=1}^{n} A_e W_i\, f(L_{1i}\, L_{2i}\, L_{3i})$$

where A_e is the area of the element, and data for the weighting coefficients W_i and area coordinates L_{1i}, L_{2i}, L_{3i} associated with n=7 sampling points are presented in Table A2.

Table A2: The values of the weighting coefficients and area coordinates.

i	W_i	(L_{1i}, L_{2i}, L_{3i})	
1	0.225	(α,α,α)	$\alpha = 1/3$
2	0.13239415	(β,γ,γ)	$\beta = 0.05971587$
3	0.13239415	(γ,β,γ)	$\gamma = 0.47014206$
4	0.13239415	(γ,γ,β)	$\delta = 0.79742669$
5	0.12593918	$(\delta,\varepsilon,\varepsilon)$	$\varepsilon = 0.10128651$
6	0.12593918	$(\varepsilon,\delta,\varepsilon)$	
7	0.12593918	$(\varepsilon,\varepsilon,\delta)$